POLITECNCICO DI TORINO

MASTER's Degree in AEROSPACE ENGINEERING

MASTER's Degree Thesis

Development of optical sensors with FBG for vibrational analysis

Supervisors

Prof. MATTEO D.L. DALLA VEDOVA

Prof. PAOLO MAGGIORE

Ing. GAETANO QUATROCCHI

Candidate

ANTONIO MAROTTA

DECEMBER 2022

Summary

The detection and study of vibrations play a fundamental role in the monitoring and safety of major engineering systems. This is especially true in the aerospace sector where the operating environment is hostile and the constraints on weights and dimensions are extremely tight. For these reasons, the research and use of sensors based on optical signal transmission are becoming increasingly important. The opportunity to implement distributed measurements along a single fibre, the small size and weight and the high resistance to electromagnetic interference make this technology an ideal candidate for the development of next-generation aerial platforms. In this paper, the operating principles and main concepts behind optical signal transmission are introduced, with particular emphasis placed on the type based on Fibre Bragg Grating (FBG). The objective is to better understand the main merits and shortcomings of this solution, for vibration sensing, and the creation of possible designs to be realised for subsequent study in the laboratory. This is done through a careful literature search and a classification of the main existing architectures. Subsequently, a possible device capable of compensating for the major problems of this solution is proposed, and the dynamic and sensitivity characteristics of the sensor are studied. A great deal of attention is paid to the properties of the support on which the fibre is to be placed, as this has a very important effect on the sensing performance. This is possible thanks to the mathematical modelling of the problem and the implementation of a Matlab script capable of estimating dimensions, weights and dynamics performances then verified through FEM modelling.

Table of Contents

List of Tables

List of Figures

Chapter 1

Fiber Optic

1.1 General Overview

Fiber Optic is the most widely used means in the field of optical communications. This type of technology is based on the use of light as a form of energy that is modulated and subsequently propagated, through the use of fibre, from source to destination. This simplifies the modulation of high-speed signals and minimises signal degradation on lines characterised by large distances. For this reason, in the last 30 years, their use has increased considerably in the telecommunications sector and has also found a place in the medical, lighting and various engineering applications.

The operating concept on which optical fiber is based is the principle of total internal reflection, the phenomenon whereby a wave propagating along the interface between different media changes direction due to the different refractive index. This latter parameter, which plays a fundamental role in the physics of the phenomenon, is a dimensionless quantity that evaluates the decrease in the propagation speed of electromagnetic radiation. It is defined as:

$$n = \frac{c}{v} \tag{1.1}$$

where:

- c is the speed of light in vacuum;
- v is the speed of light in the medium considered.

In general, the structure of the optical fibre consists of three concentric layers as shown in figure (1.1). They can be classified as:

- Core;

- Cladding;
- Coating.

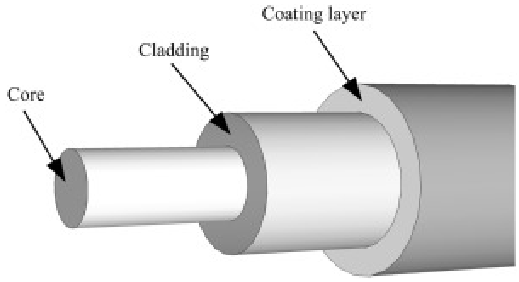

Figure 1.1: Structure of optical fiber

	Diameter
Core	$9\mu m$, $50\mu m$ or $62.5\mu m$
Cladding	$125\mu m$
Coating	$250\mu m$

Table 1.1: Principal dimensions

The outermost layer is called the coating, generally obtained from polymeric materials, and is used to isolate the innermost layers from the external environment and mechanical stresses. The innermost layer, on the other hand, defined as the core, has the task of 'guiding' light, which is achieved by appropriately combining its refractive index with that of the cladding, the intermediate layer characterised by a lower n. Generally, the most commonly used material is silica, suitably combined with other chemical compounds to improve and modify the optical and physical properties. Other materials such as plastics, heavy metal fluoride but also crystals, such as sapphire, have been used in specific applications.

Depending on the diameter of the core and its optical characteristics, different propagation modes with different attenuation and scattering values can be defined. The propagation mode defines the possible configurations in which the energy of an electromagnetic field propagates within a transmission line. It is possible to classify fibres as:

- Single-mode Step Index: the diameter of the core is very small compared to that of the cladding and it is made of glass. Single-mode propagation is only possible above a specific wavelength or Cutoff-wave, and the beam of light passes through the fibre without reflections and modal dispersion resulting in lower losses and higher bandwidth. It can only be used with laser sources, and is also the most expensive architecture and therefore used mostly for distant transmission lines.

- Multi-mode Step Index: the diameter of the core is larger, which allows for more propagation modes. This, due to the bouncing rays dispersing in the cladding, leads to high losses and also the waves do not all reach the end of the cable at the same time. They are, however, inexpensive and the larger size of the core makes them easier to use. As in the previous case, the refractive index of the core is uniform and slightly higher than the one of the cladding.

- Multi-mode Graded Index: in this case, the refractive index is not characterised by a sharp discontinuity between core and cladding but decreases in a gradual manner allowing for less modal dispersion and less output loss. They represent a compromise between single-mode and multi-mode step index.

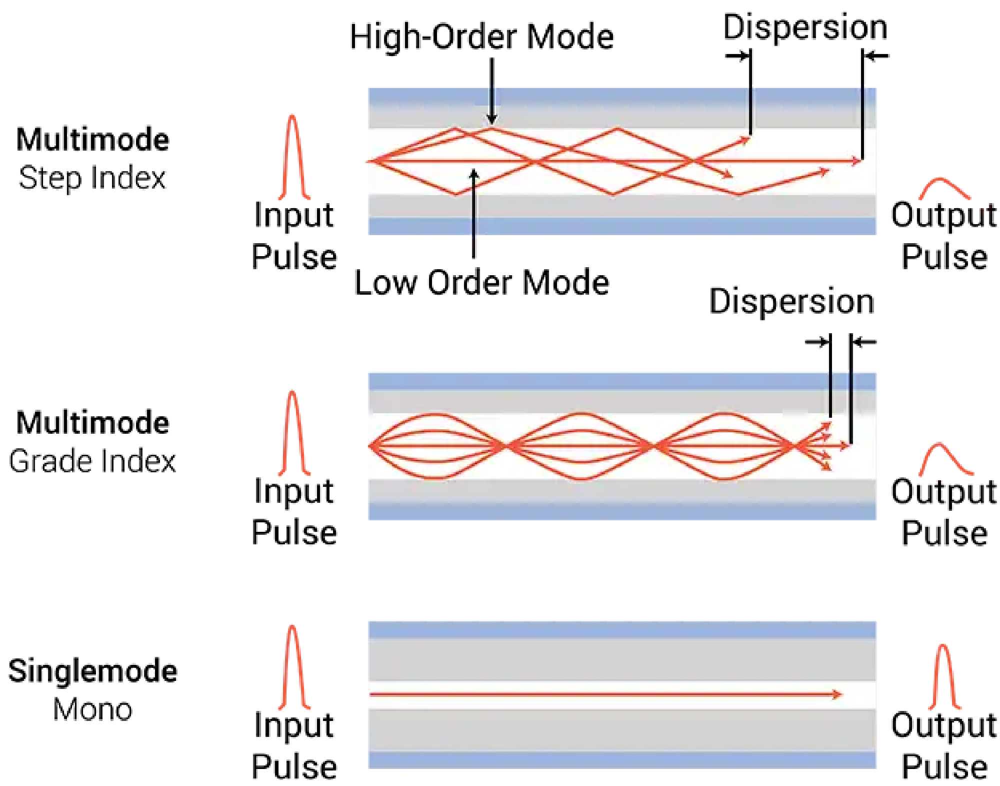

Figure 1.2: Propagation modes

1.2 Operating Principle

The principle behind the propagation of light through the fibre, as mentioned in the previous paragraph, is the concept of Total Internal Reflection, TIR. This optical phenomenon which occurs in the passage of light between mediums with different indices of refraction is well described by Snell's Law, derived from the refraction phenomenon described in the figure (1.3):

$$n_i \sin(\theta_i) = n_r \sin(\theta_r) \tag{1.2}$$

with:

- n_i: refraction index of the first material;
- n_r: refraction index of the second material;
- θ_i: incidence angle;
- θ_r: refraction angle.

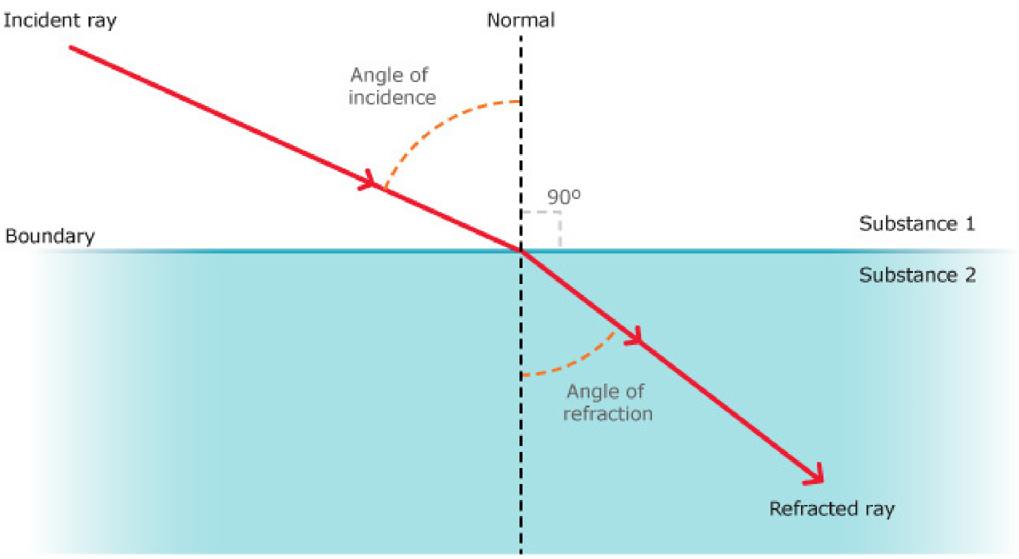

Figure 1.3: Refraction of light

Using this mathematical relationship, it is then possible to calculate the direction of the light ray at the interface between the two different materials, knowing the indices of refraction and the initial angle of incidence. Within fibre optics, the objective is to achieve a signal that is totally reflected when it encounters the discontinuity that exists between the optical properties of the core and cladding. Total reflection occurs when the angle θ_r is equal to $\frac{\pi}{2}$, at this point, by substituting this value within the formula (1.2) it is possible to calculate the angle of incidence θ_i, the critical angle:

$$\theta_i = \arcsin(\frac{n_r}{n_i}) \tag{1.3}$$

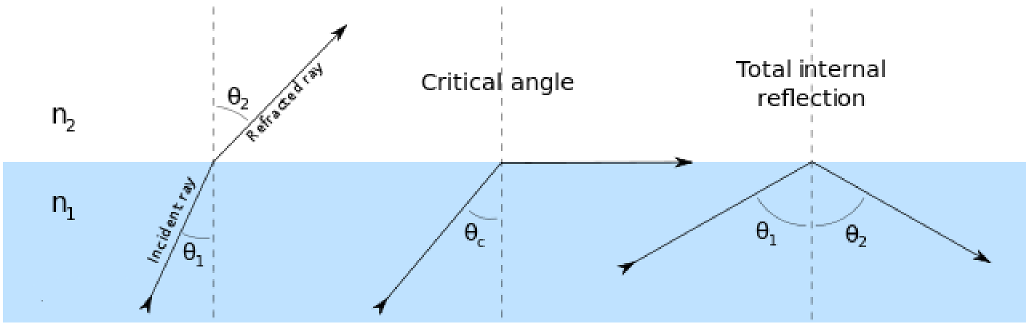

Figure 1.4: Total Internal Reflection

However, the interface with the external environment of the fibre must also be accounted for, as the beam in fact originated outside of the cable. It is then again necessary to use Snell's formula between the external environment interface, in this case, air, and the core. The equation shows that to obtain total reflection inside the core the direction of the incident ray must be contained within the so-called "acceptance cone".

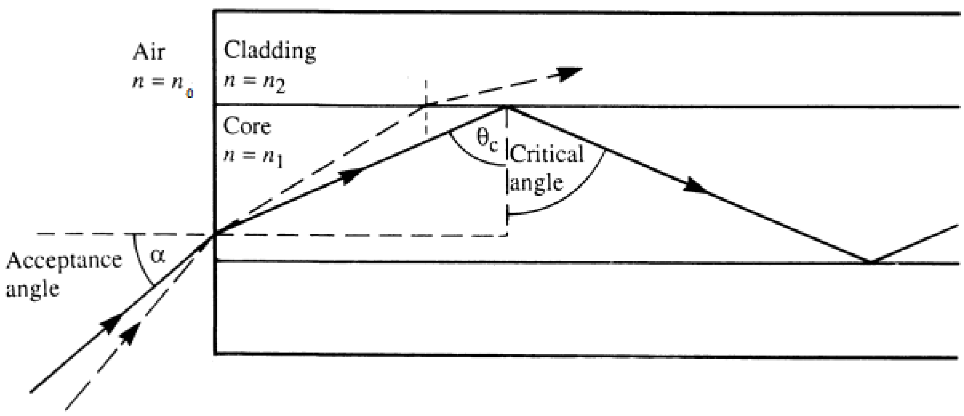

Figure 1.5: Acceptance cone

Considering the scheme in the figure (1.5), the cone half angle, α_{max} can be calculated in the following way:

$$n_0 \sin(\alpha) = n_i \sin(\frac{\pi}{2} - \theta_i) \tag{1.4}$$

where n_0 is the refractive index of the air and α the angle of incidence. Isolating the sine gives:

$$\sin(\alpha) = \frac{n_i}{n_0} \cos(\theta_i) \tag{1.5}$$

By reworking the expression and squaring the two members:

$$\cos(\theta_i) = \frac{n_0}{n_i} \sin(\alpha) \tag{1.6}$$

$$\cos^2(\theta_i) = \frac{n_0^2}{n_i^2} \sin^2(\alpha) = 1 - \sin^2(\theta_i) \tag{1.7}$$

Considering θ_i in the critical case, using the expression (1.3):

$$n_0^2 \sin^2(\alpha_{max}) = n_i^2(1 - \frac{n_r^2}{n_i^2}) \tag{1.8}$$

The angle of the cone is therefore:

$$\alpha_{max} = \arcsin\left(\frac{\sqrt{(n_i^2 - n_r^2)}}{n_0}\right) \tag{1.9}$$

The coefficient $\sqrt{(n_i^2 - n_r^2)}$ is defined as Numerical Aperture, NA:

$$\alpha_{max} = \arcsin\left(\frac{NA}{n_0}\right) \tag{1.10}$$

1.3 Performances and Drawbacks

It is safe to say that optical fibres have revolutionised the world of network communication, but their peculiarities allow them to be implemented in various sectors among which the military and aerospace where their use is set to grow. This is also evident from fig (1.6), which is based on the research conducted by [1]. Obviously, like all solutions, the use of this technology demands compromises, so to gain a better understanding of the strengths and disadvantages associated with it, it's useful to outline them below:

- Large Bandwidth: they are built to carry the signal over much greater distances than traditional cabling, offering lower power losses. In general, they are characterised by a signal loss of 0.2 [dB/Km] and bandwidths, considering coaxial cables, of approximately 400 [MHz/km].

- Thin and Lightweight: the cables are much thinner and lighter than traditional copper cables, and also more convenient to use in places where space is tight due to their small diameter.

- Superior Carrying Capacity: again due to their small size more fibres can be used in a cable of a given diameter.

- Less Interference: optical fibre cables do not carry an electrical signal but a beam of light, which makes them extremely resistant to electromagnetic interference, EMI. This allows for a very low error rate and also improves the cable's ability to transfer data over long distances without suffering noticeable signal degradation. Finally, unlike electrical signals, the light of one fibre does not interfere with that of the others.

- High-Level Security: by not radiating electromagnetic energy, it is definitely a system that offers high data security.

- Flexibility and Maintenance: the fibre is light and flexible as well as having very good resistance to high temperatures and to the effects of extreme environments such as corrosion. In addition, there is no risk of sparks making this technology ideal for use in the most demanding environments.

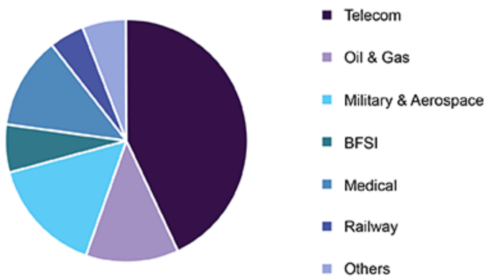

Figure 1.6: Global Fiber Optic market share

On the other hand, it is essential to bear in mind the difficulties that arise with the use of fibre optics:

- Fragility: being overwhelmingly made from fibreglass, the cables are very fragile, especially in the presence of bending.

- Splicing and Installation Difficulties: due to the smaller size and the necessary use of precision equipment the installation and splicing of fibres is an expensive and extremely delicate process.

- Data Conversion and Detector: the transmitted signal must be converted from optical to electrical and vice versa if in contact with other systems. Also, the use of a detector to handle the light signal is essential.

Finally, it is useful to mention the main factors contributing to the mechanisms of signal attenuation and dispersion within the optical fibre. Ideally, fibres are a perfect transmission medium, practically immune to external interference. However, certain physical phenomena intervene which nevertheless cause power attenuation, evaluated in [dB/Km], along the fibre:

- Intrinsic properties of the medium.
- Presence of impurities within the material and manufacturing defects.
- Losses due to the geometry and specifically the curvature but also discontinuities and deformation of the fibre itself.

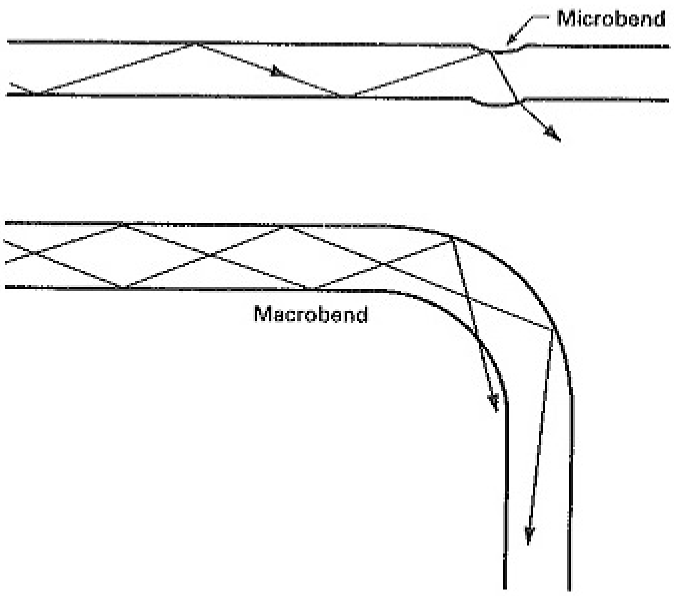

Figure 1.7: Power Loss due to Micro and Macro-Bending

In the same way, it is possible to classify the main factors determining signal dispersion. This occurs particularly at high frequencies and over long distances causing distortion and interference of the received signal.

- Modal: due to the non-synchronous arrival of the different beam modes, worsens as frequency increases.

- Chromatic Dispersion: the light beam is never perfectly monochromatic, so the resulting light beam is subject to the phenomenon described in the point above.
- Polarisation Dispersion: due to the asymmetries of the cylindrical core and the internal distortions of the fibre.

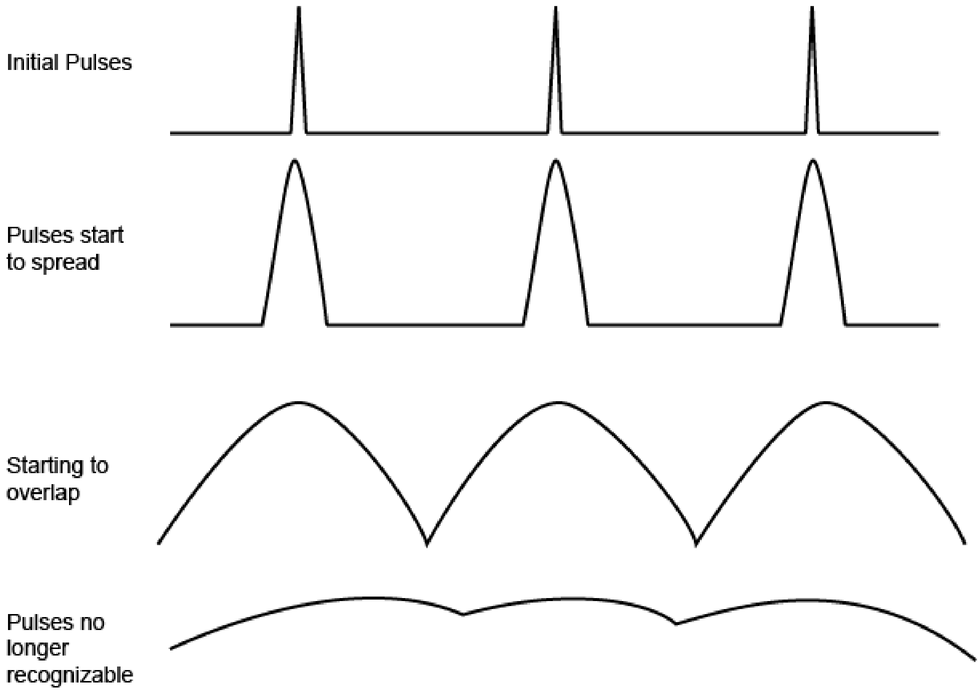

Figure 1.8: Effect of dispersion on a signal

Chapter 2

Optical Sensor and FBGs

The use and subsequent success of fibre optics in the communications sector have also enabled its implementation in the aerospace and military sector in greater depth. Proof of this is the advent of control systems with Fly By Light, FBL, architecture, which thanks to the use of optical data transmission distinguishes itself from traditional solutions by its smaller size and weight, large bandwidths and, above all, its natural resistance to electromagnetic interference. These characteristics make it an ideal candidate for next-generation aircraft, designed to meet the new challenges posed by improved electronic warfare equipment in increasingly hostile operating environments. In addition, fibre optics can measure, and thus provide information, about the environment to which they are exposed. Their application as sensors has become very popular in recent years as they can provide information such as temperature, pressure, vibration, stress and deformation. Knowledge of these values is essential in a myriad of applications, especially aerospace where components are required to operate in extreme environments. In addition, their application is essential in the future field of smart structure or system diagnostics and prognostics.

2.1 Optical Sensor Architectures

The values measured by the fibre optic detectors are obtained through the precise study of the characteristics of the sensor output, i.e. light. It is in fact possible to obtain mathematical models that relate variations in, for example, the wavelength of the beam to the physical phenomena to which the sensor is subjected. There are various kinds of solutions, the first major categorisation that can be identified is given below with a table that summarises the measurable physical parameters:

- Intrinsic (Direct) Sensor: the physical phenomenon to be measured modifies and thus modulates the characteristics of the beam along the fibre, varying intensity, polarisation, phase and wavelength. This architecture is the most basic as it allows measurement using simply the fibre source and the associated detector. A particular advantage of this solution is the possibility of obtaining a distributed configuration that allows the ability to measure along the entire length of the fibre.

- Extrinsic (Indirect) sensor: in this case, the task of the cable is to transmit the light beam, multi-mode, from an electrical or more generally non-optical sensor connected to an optical transmitter. The fibre is only used for data transmission and the light modulation is carried out by an external sensor. The advantage of this type of architecture is the possibility of reaching small and hostile spaces.

Temperature
Pressure
Deformation
Displacement
Vibration
Humidity

Table 2.1: Measurable physical parameters

Finally, it is useful to mention the main elements that make up the optical sensor system. First and foremost, the light source, which may be LED or laser, runs the length of the fibre and is subject to the effects of the external environment. Using the cable's own sensing element or external transducer, it is possible to modulate the beam which is then collected by the detector. There are many possible sensor types and architectures that can be implemented, but this work will focus exclusively on the solution based on Fiber Bragg Gratings or FBGs discussed in more detail in the next section.

2.2 FBGs

FBGs are one of the main solutions used in the construction of optical sensors. They are based on the concept of Bragg Grating, a micro-structure within the optical fibre core characterised by multiple layers with varying refractive indexes. This causes partial refraction of the light beam, i.e. a specific wavelength is refracted while the remaining energy packet is allowed to pass through. The periodicity of the grating is what defines the reflected wavelength and it is the change in this periodicity, under the action of external agents, that allows the phenomenon to be measured. In addition to possessing all the qualities listed previously, this type of sensor allows, with the use of a single fibre, a distributed measurement over its length.

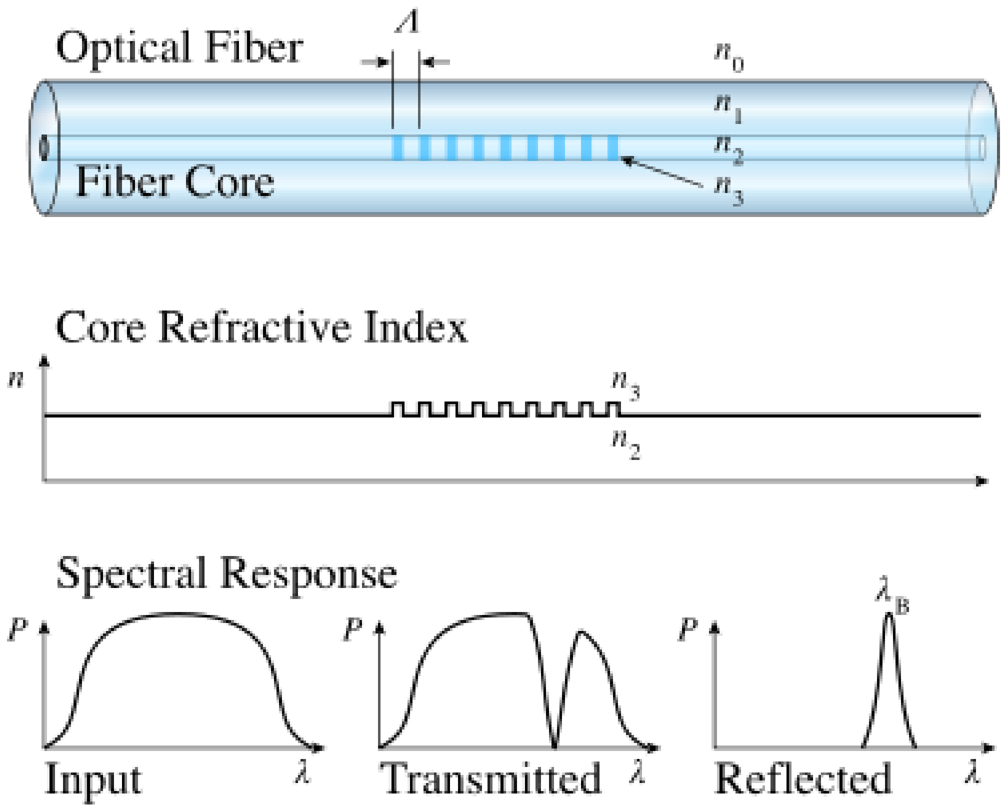

Figure 2.1: FBGs structures and principles

Bragg grating, therefore, acts as a filter for the wavelength of the beam within the fibre. It is based on the physical principle of Fresnel Reflection according to which when light passes through a medium with different refractive indexes, it can be both refracted and reflected. The wavelength reflected, as shown in figure (2.2), is characterised by the so-called Bragg Wavelength which corresponds the energy peak of the wave. The fundamental relationship that describes its behaviour is as follows:

$$\lambda_B = 2n_{eff}\Lambda \tag{2.1}$$

where:

- n_{eff}: is the effective refractive index of the grating;
- λ_B: is the Bragg Wavelength;
- Λ: is the period of the grating.

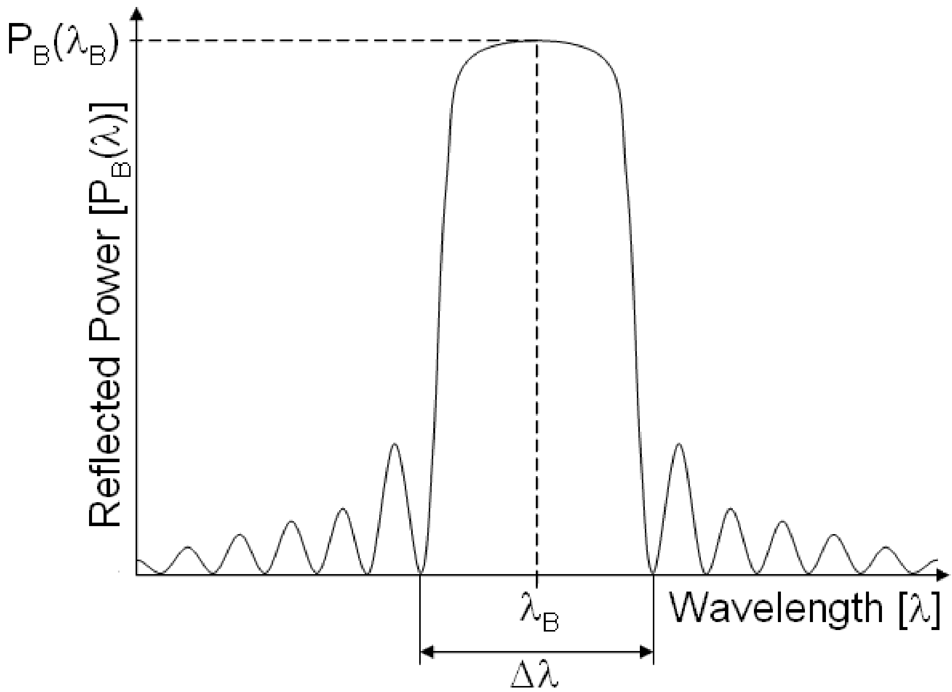

Figure 2.2: Reflected Wavelength characteristic

So it is precisely the alteration of these parameters describing the geometry and the optical properties of the grating that allows its use as a sensor, whose task is to capture variations in the reflected wave and link them through a mathematical model to the physical quantities of interest.

2.3 Gratings Structures

The internal structure constituting the grating can have different configurations depending on the variation of refractive indices and grating period. The six most commonly used configurations are as follows:

- Uniform Grating: refractive index and period variation are constant with only positive index variation.
- Gaussian/Raised Cosine Apodized Grating: in which the refractive index variation follows a certain mathematical function.
- Chirped Grating: while the refractive index remains constant, there is a linear variation of the grating period.

- Tilted Grating: the variation of the refractive index does not follow the fibre axis, or optical axis, but has a certain angle to it.
- Long Period Grating: typically, the grating period is of the same order of magnitude as the Bragg Wavelength (500-1500 [μm]). By increasing the size, up to 1 [mm], it is possible to simplify its construction and increase its response.
- Phase Shifted Grating: obtained by dividing a standard FBG into two identical ones but with a phase difference corresponding to half a period, this creates an interference that allows for a very narrow transmission band in the centre of the spectrum.

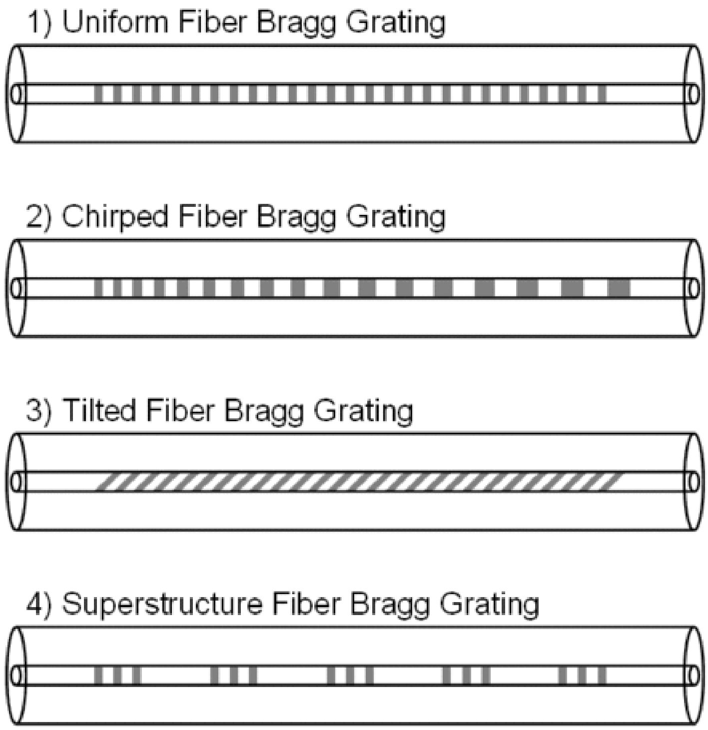

Figure 2.3: Different gratings structures

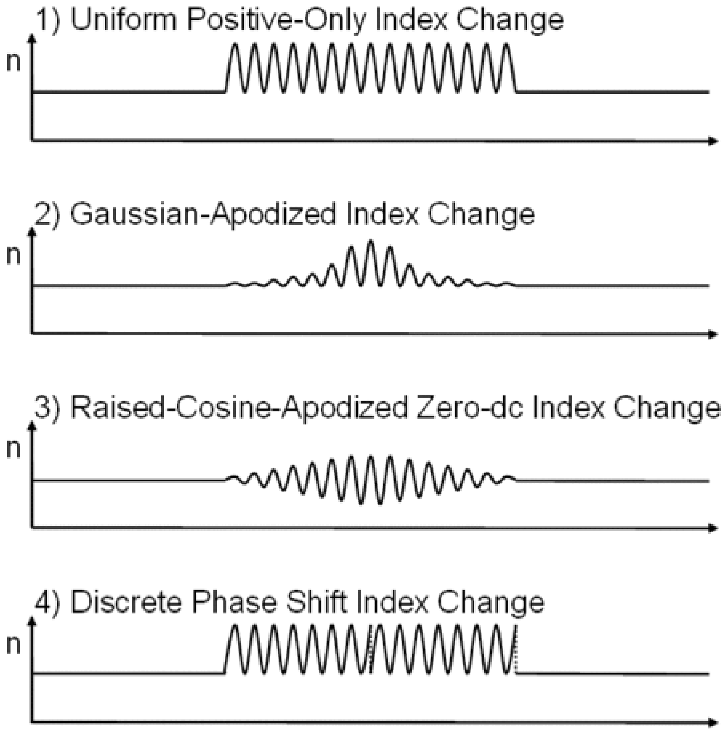

Figure 2.4: Index variation

2.4 FBG Mathematical Model

Environmental conditions, primarily temperature and humidity, have a considerable effect on the output of the FBG. Humidity in the air can bring vapour particles into the coating producing a deformation of the fibre and resulting in a variation of the reflected wave. The main influence, however, is that of temperature variations which have an effect on both the refractive index and the grating period due to thermal expansion/contraction. The goal of this section is to obtain a mathematical relationship that relates the Bragg Wavelength variation with alterations in ambient conditions and, of course, the external loads to be measured. To do this, one differentiates the constitutive equation (2.1) with respect to strain and with respect to temperature:

$$\frac{\Delta\lambda_B}{\lambda_B} = \frac{\Delta(n_{eff}\Lambda)}{n_{eff}\Lambda} = \left(1 + \frac{1}{n_{eff}}\frac{\delta n_{eff}}{\delta\varepsilon}\right)\Delta\varepsilon = (1 + p_e)\Delta\varepsilon \tag{2.2}$$

$$\frac{\Delta\lambda_B}{\lambda_B} = \frac{\Delta(n_{eff}\Lambda)}{n_{eff}\Lambda} = \left(\frac{1}{\Lambda}\frac{\Lambda}{\delta T} + \frac{1}{n_{eff}}\frac{\delta n_{eff}}{\delta T}\right)\Delta T = (\alpha_\Lambda + \alpha_n)\Delta T \tag{2.3}$$

At this point, the constitutive model of the sensor can be obtained:

$$\Delta\lambda_B = \lambda_B(1 + p_e)\Delta\varepsilon + \lambda_B(\alpha_\Lambda + \alpha_n)\Delta T \tag{2.4}$$

Where:

- λ_B is the Bragg reflected wavelength;
- p_e is the strain-optic coefficient of the fiber;
- $\Delta\varepsilon$ is the variation of the fiber strain;
- α_Λ is the thermal expansion coefficient;
- α_n is the thermo optic coefficient;
- ΔT is the variation of temperature.

The equation can be rewritten by introducing two coefficients:

$$\Delta\lambda_B = K_\varepsilon\Delta\varepsilon + K_T\Delta T \tag{2.5}$$

which are defined as:

- $K_\varepsilon = \lambda_B(1 + p_e)$ is the strain optic coefficient, it depends from the material of the fiber and relates the change in the refractive index of the grating to the normal deformation. It is considered $p_e = -0.212$.
- $\lambda_B(\alpha_\Lambda + \alpha_n)$ is composed of the thermo-optical factor, which links temperature variation with refractive index variation, and a thermal expansion contribution. This term will not be taken into account in the following sections due to the compensatory measures that have been considered.

2.5 FBG Fabrication's Methods

FBGs are most commonly manufactured using "germanium-doped" silica, a photosensitive material whose refractive index of the core can be changed by exposing it to ultraviolet light. The change in optical properties depends on the intensity and time of UV exposure. The grating is thus obtained by predefined, periodic/aperiodic, modification of the index of refraction of the fibre through two main methods, interference and masking:

- Interference: this is the first method used for the production of FBG. UV beams are produced by a laser source that is split and made to interfere to create the desired pattern for grating. This method makes it possible to change the Bragg wavelength rapidly, the latter being a function of the laser wavelength and the geometry produced by the lenses used, figure (2.5).

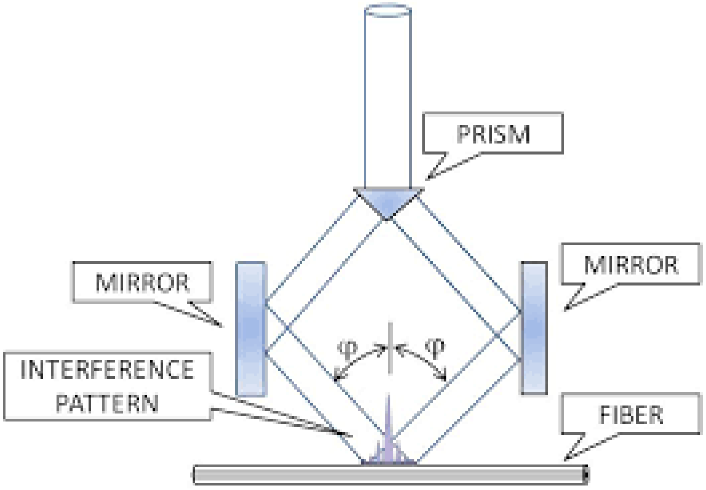

Figure 2.5: Interferometer method

- Phase Mask Method: the creation of the pattern is achieved through the use of a photo-mask which has the desired grating characteristics. This is placed between the ultraviolet source and the fibre, the shadow produced activates the photosensitive properties of the fibre producing the desired FBG.

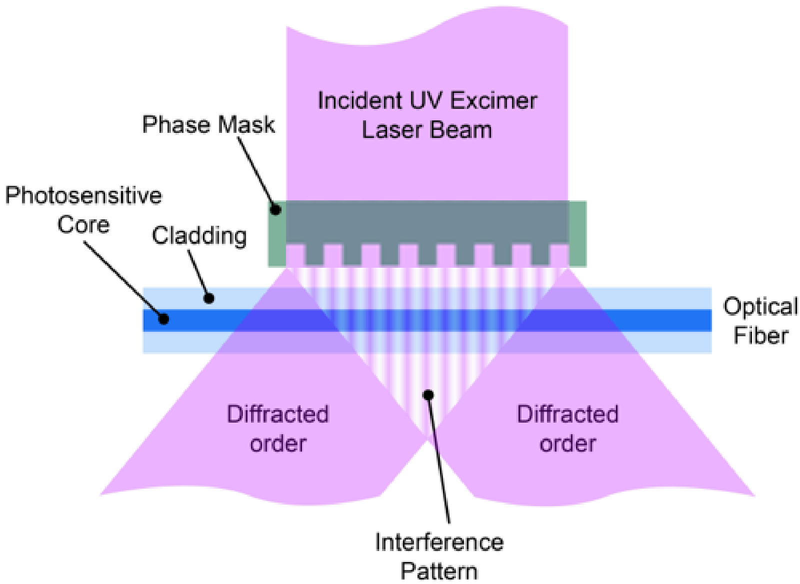

Figure 2.6: Photo-mask method

- Point by Point: a laser with a highly concentrated beam is used to "write" the grating point by point.

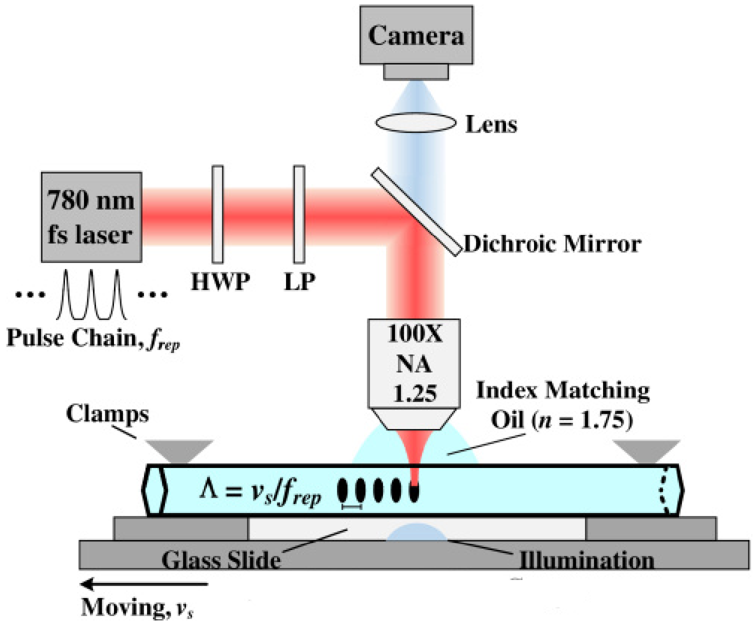

Figure 2.7: Point by Point method

2.6 Aerospace Applications

In conclusion, it can certainly be said that optical fibre is a necessary technology for the development of sensing and monitoring techniques for the aerial platforms of the future [2]. These are characterised by the use of an incredible amount of data, which is manipulated through the BUS structure. In aerospace applications, fibre buses allow the handling of up to 40 [Gb/s] of traffic volume, with much lower losses than traditional cables. This solution allows the implementation of new measurement techniques with the potential to significantly improve the diagnostic and prognostic capabilities of the systems. It allows downtime to be reduced and greater availability of the platform due to the implementation of predictive maintenance. The decrease in weight, the high amount of data transmission and the high resistance to external agents make fibre optic sensors ideal candidates for new control systems, especially those used in engine management where high temperatures and tight spaces require great compromises to traditional sensors. The possibility of creating on a single fibre a network of distributed sensors enables monitoring of the stresses and strains the structure is subjected to, knowledge of these values is essential for improving aircraft safety, especially in the area of fatigue, and for the optimization of the maintenance operations. In the space sector too this solution is showing promise, especially considering the hostile environment to which space missions are often subjected, involving high-temperature gradients and constant exposure to electromagnetic radiation.

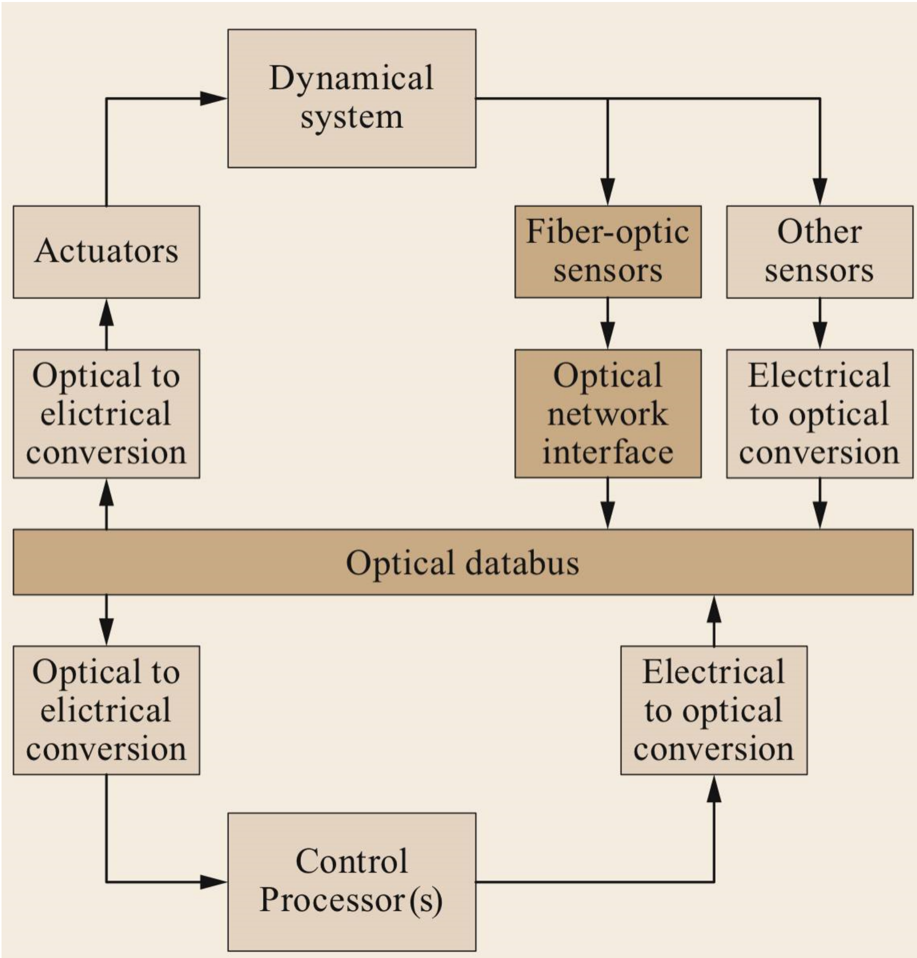

Figure 2.8: Example of Control System Architecture based on optical network

Chapter 3

FBG Vibration Sensors

3.1 Vibration

Vibration measurement plays a key role within modern engineering systems as it ensures their safety and proper functioning. In most cases, abnormal behaviour or damage in these systems results in unwanted vibrations which can then be used as an alarm bell or diagnostic tool. For this reason, the sensors used in this sector provide monitoring of a component's state of health, preventing the occurrence of faults. The typical architectures used in these areas are based on capacitive or piezoelectric technology. Although inexpensive and generally very accurate, these technologies are not able to cope with the most extreme operating environments where external electromagnetic interference is present and furthermore distributed measurement is impossible. For these reasons, in addition to those already listed in the previous sections, the implementation of FBG sensors is becoming increasingly popular in this field. FOVS, fibre optical vibration sensors, can be classified into three different categories, depending on the principle of demodulation they use:

- Intensity demodulation based: characterised by low cost and high bandwidth but is plagued by high measurement instability due to fibre bending and power fluctuations.

- Interferometric demodulation based: can provide accurate and stable measurements but have bandwidth limitations and measurement operations are much more expensive and complicated.

- Wavelength demodulation based: which is the operating principle of FBG-based FOVS and is characterised by the ability to obtain distributed measurements as well as being intrinsically resistant to light intensity fluctuations and losses due to fibre bending.

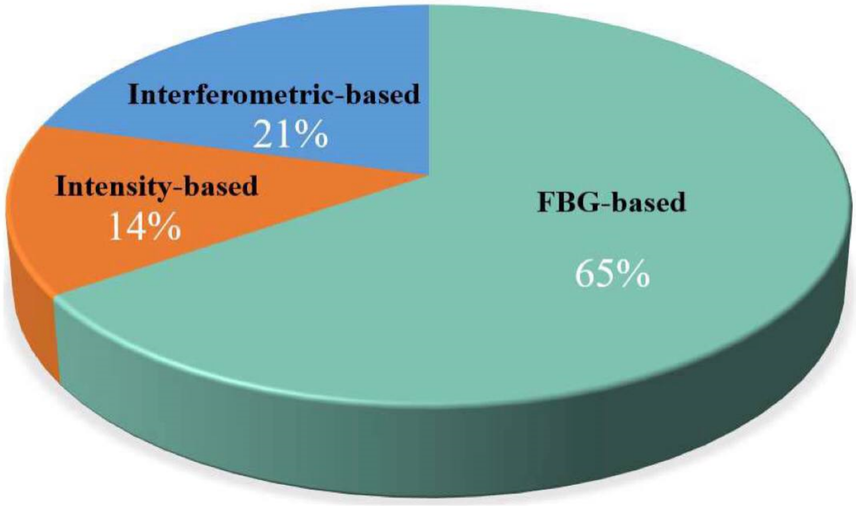

Figure 3.1: Percentage Chart of different type of FOVS in literature

It is no coincidence that it is precisely the latter that has received the most attention in recent years, covering as much as 65% of all the literature produced on the subject of FOVS within the Academic Web of Science database [3]. As shown by equation (2.5) the FBG can sense axial stress along its length, which is why supports are required to convert the vibration signal into the axial deformation of the fibre. Typically, the support and fibre can be modelled as a mass-spring-damping system from which one can then obtain the performance and range of application of the sensor. These values are extremely sensitive to the type of mount used, which therefore plays a fundamental role in defining the measurement range of the sensor, i.e. in defining a working zone where no signal distortion occurs.

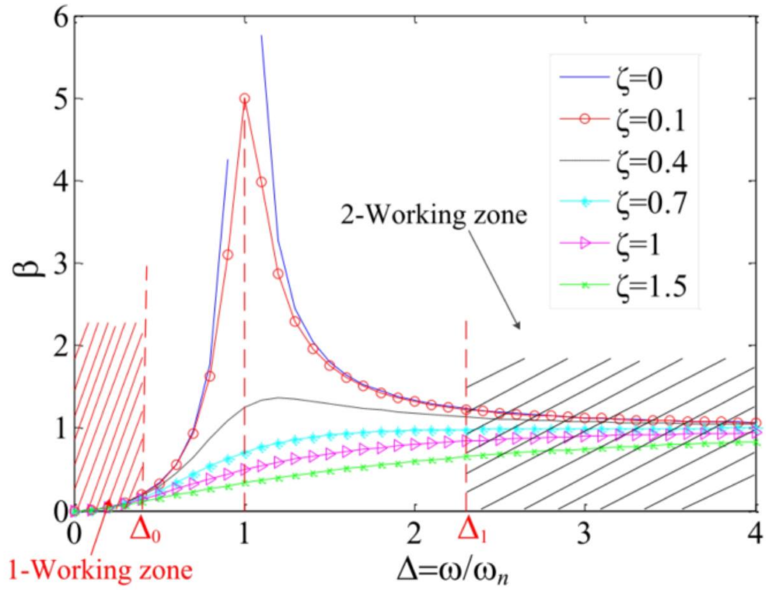

Figure 3.2: Amplitude-frequency response of a second order system

3.2 Sensors Architectures

In recent years, the development of this technology has led to the emergence of numerous proposals for FBG-based vibration sensors. Depending on how vibration and fibre strain are linked, it is possible to identify three different architectures, namely pasted FBG-based [4] [5], axial property of FBG-based [6] [7] and transverse property of FBG-based [8] [9].

In the pasted type, the sensor converts the vibration into the deformation of the elastic support, which through adhesive is transmitted to the FBG. This is certainly the most used, as it is characterised by a simple mathematical model and an easy-to-build support structure, which is usually a single component such as a cantilever beam that can be easily realised in 3D, thus making prototyping immediate. The greatest difficulties are encountered in the realisation of the bonding and in determining its properties. It is very difficult to estimate the load transfer factor, which depends not only on the type of glue used but also on the environmental effects, the ageing of the substance and the bonding geometry. Furthermore, great attention must be paid to the Chirping phenomenon, which is particularly present in this type of solution. This effect occurs when the deformation of the support and consequently that of the fibre is not uniform along its length, which causes a non-uniform variation of the grating geometry and effective refractive index. The signal measured will consequently be distorted, preventing the sensor from functioning correctly.

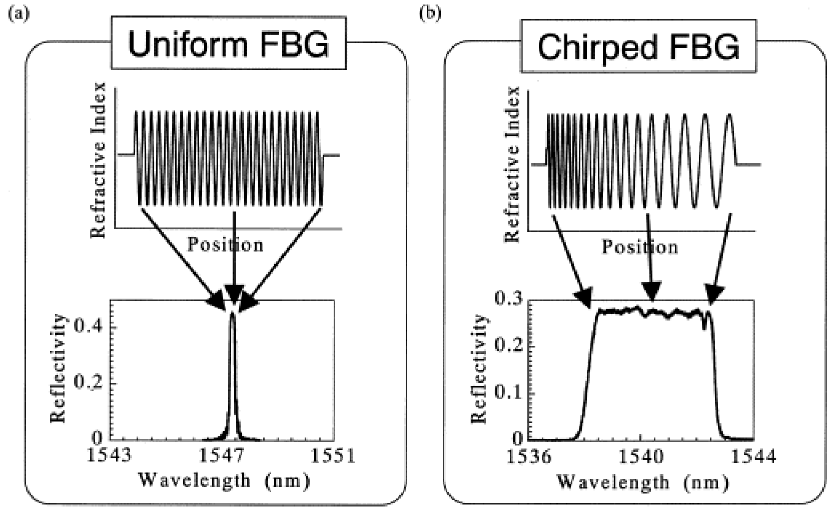

Figure 3.3: Chirp effect on the FBG output and properties

Figure (3.3) shows the effect on the reflected Bragg Wavelength and the change in the refractive index due to chirping, it is evident how the distortion of the signal affects the goodness of measurement which is extremely sensitive to the peak value of λ_B.

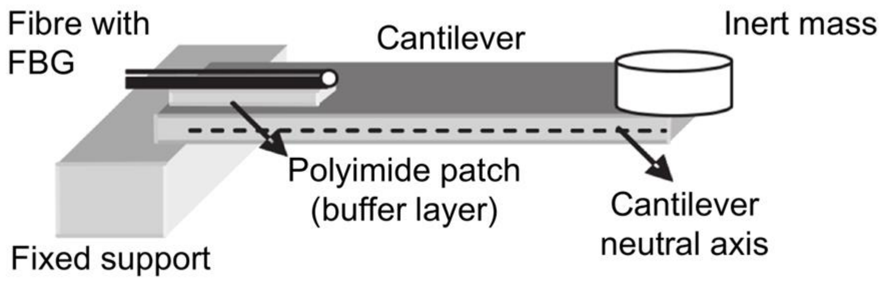

Figure 3.4: Pasted FBG-based solution

The type of sensor based on the axial property, on the other hand, is generally featuring an FBG suspended and constrained at the extremes. The vibration is transferred to the fibre due to the inertia of a mass and then converted into a compressive or tensile deformation along the filament axis. This allows an improvement of the sensing properties and the elimination of the chirping effect. However, they are characterised by low sensitivity due to the high axial stiffness of the glass. The fabrication of the support is more complicated than the pasted solution, generally requiring more components or components with more complicated shapes and mathematical modellings such as the coupling of two L-shaped cantilever beams or the use of diaphragms. Furthermore, the effect of vibrations along non-axial directions is not taken into account, but this has an effect on the output of the sensor and requires special measures to limit its influence.

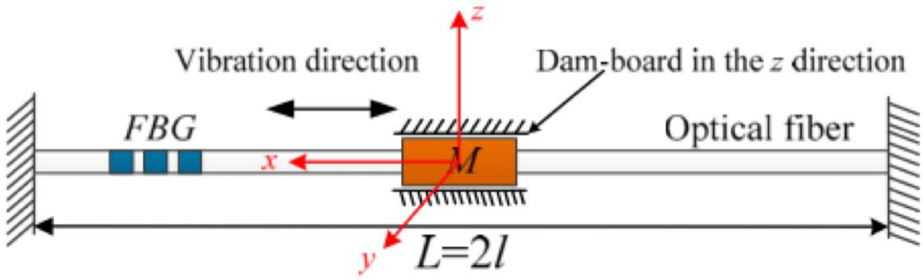

Figure 3.5: Axial FBG-based solution

The last category is instead based on the transverse properties of the fibre, similar to the previous architecture the FBG is suspended and constrained at the ends but in this case, the inertial force acts along the transverse direction. This allows the compression or traction of the grating to be amplified, achieving greater sensitivity than the axial solution. The performance obtained is certainly the best when compared to the pasted and axial solutions, but this entails a great complication in the realisation of the support structure. These in fact consist of many more components and require much more complex tolerances and geometries. Consequently, the mathematical model to be implemented is also very tricky, as is the definition of the sensor's working zone. Transverse deformation can generate distortions in the output signal and must therefore be handled very carefully.

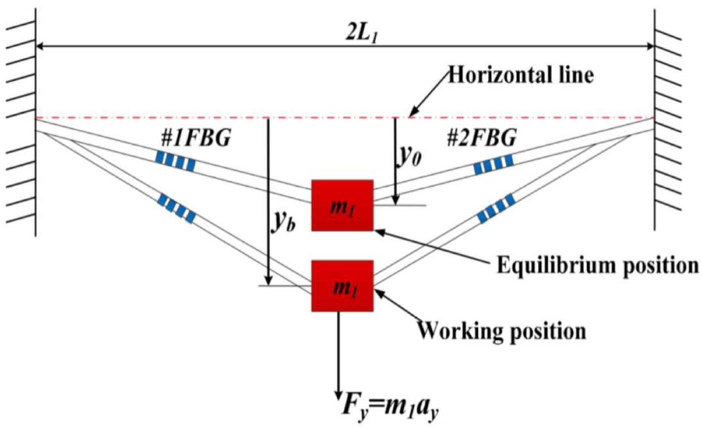

Figure 3.6: Transverse FBG-based solution

3.3 Demodulation

The fundamental component that allows the sensor to function properly is the demodulator or interrogator [10]. This has the role of obtaining the measurement from the light signal returning from the fibre and specifically the change in Bragg Wavelength. The demodulator must be able to pick up the change in wavelength and provide the correct measurement, it is essential to have high accuracy and scanning speed to obtain a sensor with good performance. Unfortunately, however, the devices on the market today are extremely expensive and unsuitable for real-world applications, outside the laboratory context, and for this reason, that new demodulation techniques have been implemented in recent years to improve the device performance [11] [12]. Some are quite simple but limited in the resolution of the measurement, dynamic range or multiplexing, while others, more complicated, improve device characteristics at the expense of cost and measurement stability. Unfortunately, however, low-cost devices with acceptable performance are still not available, severely limiting the widespread commercial use of this type of sensor. It is of fundamental importance to concentrate future efforts within this area on the realisation of affordable interrogators capable of making distributed measurements over several channels with precision and speed.

Chapter 4

Pasted FBG Sensor Design

4.1 Design Requirements

This section discusses the requirements considered for the design of a sensor for the detection of vibrations, and therefore of acceleration, based on the Pasted architecture. The objective is to realize a possible design, study its performance, and create a mathematical model capable of predicting its behaviour to obtain an instrument that can be tested in the laboratory. Precisely for this reason, it is necessary to identify and justify the most stringent requirements that dictate many of the solutions implemented. The first constraint considered is that of dimensions, which must be very small; the sensor must be capable of measuring the vibrations of the main mechanical components within an aerospace system where size and weight play a key role. This must be characterised by a good sensitivity, a value which indicates how much the output changes as the input varies. This is a crucial parameter since the greater the sensitivity the smallest change of acceleration will be felt by the sensor and more specifically by the detector that measures the Bragg Wavelength variation. The support must be characterised by a resonance frequency of 200 [Hz] or more, to guarantee a correct measurement of the most frequent vibrations within the main mechanical parts. The design considered must also be able to avoid the occurrence of the Chirping phenomenon, described in the previous section, and as far as possible compensate for the effect of temperature on the measurement. As shown by equation (2.5) the length of the reflected Bragg wave has a strong dependence on ΔT, this makes the measurement extremely dependent on changes in environmental conditions and inevitably makes the sensor both inaccurate and less precise. Furthermore, it is desired to obtain a design characterised by a few parts and easily realised with the tools available within Politecnico's laboratories. In addition, its realisation must be quickly and easily modified according to the results obtained from the experiments, possibly using a

3D printer. It is precisely for these reasons, summarised in the table (4.1), that a Pasted architecture was chosen, guaranteeing sufficient dynamic and measurement performance while using a support structure that is easy and quick to implement, without the use of expensive devices or materials. Finally, it is important to point out that with this type of architecture it is only possible to measure acceleration along one direction, it is still possible to extend the operation by considering three dimensions, but this greatly complicates the design and modelling of the component [13].

Small size
Good Sensitivity
Resonant Frequency $\geq$ 200 Hz
Chirp mitigation
Temperature mitigation
Easy to manufacture

Table 4.1: Design requirements

4.2 Support Modelling

The operating principle of the FBG pasted sensor in this case is based on the use of a mounting cantilever-type beam. The latter at the extremity features a lumped mass while the fibre is fixed by glueing it to the surface of the support. When the assembly is subjected to vibrations, the mass imposes an inertial load of modulus $F = ma$ on the cantilever beam. The bending thus generated causes compression or tensile deformation of the part then transferred, with an appropriate reduction factor due to bonding, to the fibre. This is then picked up in the form of a Bragg Wavelength variation by the detector and subsequently correlated to the value of the acceleration to which it has been subjected.

The support plays a major role in determining the performance and the proper functioning of the sensor. It defines the sensitivity, the working range, and the dynamic characteristics of the device and hence requires great consideration. The use of a support based on the cantilever beam simplifies the problem considerably as it is characterised by simple geometries and characteristic equations. Extensive use will be made of the beam model based on the Euler Bernoulli theory and for this reason, it is useful to list its main assumptions [14]:

- The shape and geometry of the beam cross-sections do not change significantly as a result of the application of transverse loads. This means that a cross-section can be assumed to be a rigid surface during deformation and can only

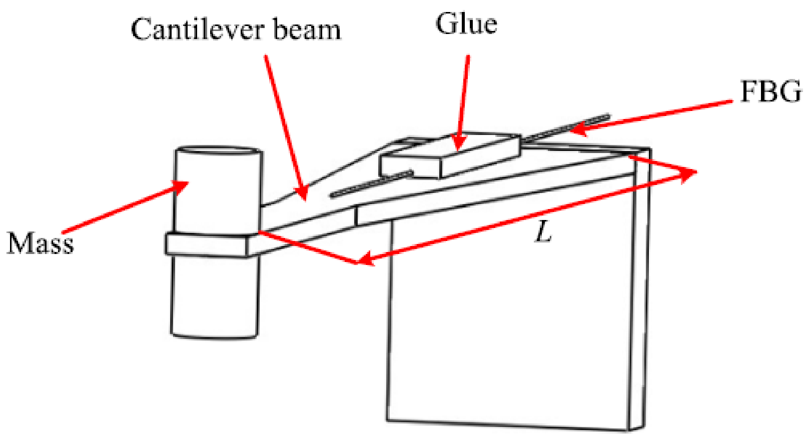

Figure 4.1: Typical Architecture of a Pasted FBG Cantilever Beam sensor

rotate.

- During deformation, it is assumed that the beam cross-section remains planar and normal to the deformed axis of the beam.
- Although the neutral axis of the beam becomes curved after deformation, the deformed angles, slopes, are small.
- The length of the beam is significantly greater than its width and thickness.

In addition, an equal-strength cantilever beam, which has equal strength in each of its sections, is used to limit the chirping phenomenon. This allows to achieve constant deformations on the support surfaces and thus avoids non-uniform deformations of the Bragg grating. A characterisation of this special geometry is carried out by introducing the constitutive equations and demonstrating its properties.

4.2.1 Equal Strength Cantilever Beam

As shown in figure (4.2), the X-axis represents the centre line of the beam, the Y-axis is the symmetry axis of the cross-section and the Z-axis is perpendicular to the two. The moment of inertia of the section of the equal-strength cantilever can be derived using the following formula:

$$I(x) = \frac{1}{12} b(x) h^3 \tag{4.1}$$

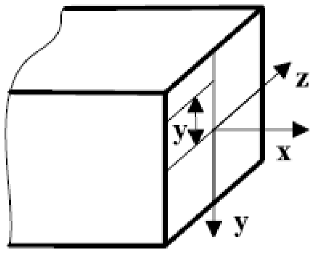

Figure 4.2: System of reference considered

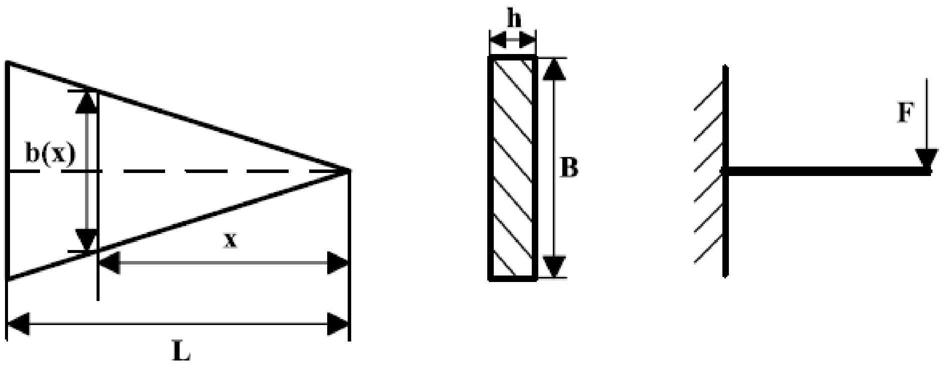

Figure 4.3: Equal Strength Cantilever Beam geometry

The resultant bending moment at section X under force F can be written as:

$$M(x) = Fx \tag{4.2}$$

Using the formulae derived from the Euler Bernoulli beam theory, it is possible to derive the stress at the desired cross section in the following way:

$$\sigma(x) = \frac{M(x)}{I(x)}y = \frac{12Fx}{b(x)h^3}y \tag{4.3}$$

At this point, it is useful to recall Hooke's law that relates deformation to stress:

$$\sigma = E\varepsilon \tag{4.4}$$

Through the latter, one can then derive the value of the general strain and maximum strain in modulus, i.e. the one present on the beam's back and belly, $y = h/2$:

$$\varepsilon(x) = \frac{12Fx}{b(x)h^3E}y \tag{4.5}$$

$$\varepsilon_{max}(x) = \frac{6Fx}{b(x)h^2E} \tag{4.6}$$

The constitutive equation defining the geometry of the equal strength cantilever can be described as:

$$\frac{x}{b(x)} = \frac{1}{2}\cot\alpha = \frac{L}{B} \tag{4.7}$$

Combining this with the maximum strain expression gives:

$$\varepsilon = \frac{6FL}{Bh^2E} \tag{4.8}$$

As can be seen, this expression is constant and depends only upon the value of the transverse force F, thus allowing constant deformation along the length of the beam and the avoidance of chirping.

Symbol	Description
E	Young Modulus
L	Full Length of cantilever beam
B	Large-end Width of cantilever beam
h	Thickness of cantilever beam

Table 4.2: Symbol Description

4.2.2 Dynamic Model

The use of the beam allows the implementation of a simple dynamic model that can be assimilated to a spring-mass system subjected to an alternating load. This is possible thanks to the use of the equations obtainable from the model of Euler Bernoulli and in considering the flexural stiffness of the structure as the stiffness of a spring with a mass at the end. The inertial force imposed by the vibrational mode is therefore considered as the external load of the mass-spring system, and the resulting dynamic properties will obviously be influenced by the geometric and mass parameters of the structure. Before doing so, however, it is useful to derive the expression describing the bending stiffness of the beam. To do this, one has to consider the model in figure (4.4) consisting of a simple cantilever beam with a rectangular cross-section subjected to the action of a transverse force F. It

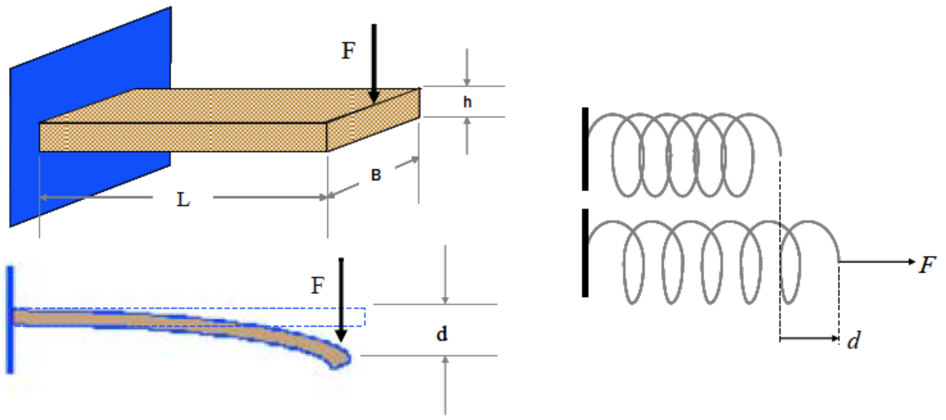

Figure 4.4: Beam and Spring modelling

is possible to link the deflection d and the external force through the following expression:

$$F = \left[\frac{3EI}{L^3}\right] d \tag{4.9}$$

Where:

- E is the elastic modulus of the material;
- $I = \frac{1}{12}Bh^3$ is the moment of inertia of the cross section;
- L: is the length of the beam.

This can be seen as the constitutive spring equation in which the force is proportional to the deformation through a coefficient K, i.e. the stiffness. It is clear that it is feasible to consider the flexural motion of the structure as a spring under the action of an external force with K equal to the flexural stiffness of the beam.

$$K = \frac{3EI}{L^3} \tag{4.10}$$

Considering the modelling just proposed, it is now time to derive the differential equation describing the kinetics of the vibrational phenomenon concentrating on the motion/deflection of the beam end, the modulus of which will be indicated as Y equal to d in figure (4.4):

$$m\ddot{Y} + K\dot{Y} = F\sin(\omega t) \tag{4.11}$$

Where:

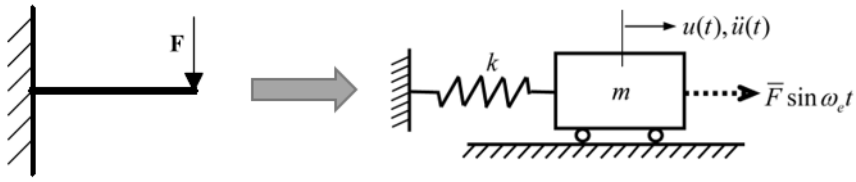

Figure 4.5: Dynamic model considered

- m = mass at beam end;
- K = flexural stiffness of the beam;
- F = external load;
- ω = frequency of the external load.

As can be seen in this case, it is preferable to neglect the structural damping of the beam in order to achieve simpler modelling. Furthermore, it is very complicated to obtain damping values for real structures, these are not constant and depend on many parameters. It is much more convenient to implement the effect within the FEM analysis and study its behaviour in the laboratory, thus considering all the factors that come into play in the realisation of the component.

Solving the differential equation (4.11) gives the value of the deflection:

$$Y = \frac{F}{m(\omega_0^2 - \omega^2)} = \frac{a}{(\omega_0^2 - \omega^2)} \tag{4.12}$$

In which:

- $\omega_0^2 = \frac{K}{m}$ is the system's inherent frequency;
- a is the acceleration to which the system is subjected.

4.2.3 Sensor Constitutive Equation

At this point, once the dynamic model has been obtained, one can link it with the equations governing the structural properties of the support to derive the constitutive equation connecting the acceleration, to which the sensor is subjected, with the Bragg Wavelength shift. By doing so, one can calculate the expression that governs the operation of the device and characterises its measurement capability, in fact, it is from this specific expression that the Sensitivity is derived. Before this, it is useful to recall the terms obtained from section (4.2.1) and in particular the value of the surface deformation of the equal strength beam and the value of the deflection at the end:

$$\varepsilon = \frac{12FLz}{EBh^3} \tag{4.13}$$

$$Y = \frac{4FL^3}{EBh^3} \tag{4.14}$$

Where:

- z: represents the distance of each longitudinal section from the neutral axis of the beam.

It is now possible to combine the (4.14),(4.13) and (4.12) equations in order to derive the relationship linking deformation with acceleration:

$$\varepsilon = \frac{3Yz}{L^2} = \frac{3z}{(\omega_0^2 - \omega^2)L^2}a \tag{4.15}$$

This can be further simplified if one consider the frequency of the external load negligible when compared to the system's own frequency, $\omega << \omega_0$:

$$\varepsilon = \frac{3z}{\omega_0^2 L^2}a \tag{4.16}$$

It is now necessary to recall the expression (2.4) obtained in the previous chapters, which describes the working principle of the FBG.

$$\Delta\lambda_B = \lambda_B(1 + p_e)\Delta\varepsilon + \lambda_B(\alpha_\Lambda + \alpha_n)\Delta T \tag{4.17}$$

At this time, the effect of temperature will be neglected and a factor will be introduced to take into account the effect of glueing. In fact, due to the bonding, the deformation of the support cannot be equal to that of the fibre, there will certainly be a loss due to the viscous movement, even if minimal, of the substance used as adhesive:

$$\Delta\varepsilon = \alpha\varepsilon \tag{4.18}$$

In which:

- $\alpha(0 < \alpha < 1)$ is defined as the glue transfer factor.

Considering this, the constitutive equation of the sensor is finally derived, which enables the acceleration applied to the system to be measured through the Bragg Wavelength shift:

$$\Delta\lambda_B = (1-\rho_e)\frac{3\alpha z\lambda_B}{\omega_0^2 L^2}a \tag{4.19}$$

4.3 Sensitivity and Temperature Mitigation

A factor that plays a major role in determining the performance of a sensor is Sensitivity. This value makes it possible to identify the smallest variation of the measurable quantity, which is why it is important to have the largest possible value. In the case study, sensitivity can be obtained by starting from the formula (4.19) and taking the acceleration to the first member:

$$S = \frac{\Delta\lambda_B}{a} = (1-\rho_e)\frac{3\alpha z\lambda_B}{\omega_0^2 L^2} \tag{4.20}$$

In essence, the sensitivity indicates how many metres the reflected wavelength varies for each g of imposed acceleration. As can be seen, however, this design does not allow high sensitivity and high frequencies, in fact, the two values are inversely proportional. This is even clearer if one observes the trend shown in figure (4.6); for clarity of exposition, the axes are in logarithmic base and also shown is the influence of the distance z, between the fibre and the neutral axis of the support. The values of the other parameters are shown in table (4.3). Above 1800 $[rad/s]$, approx. 300 $[Hz]$, the sensitivity begins to have a magnitude in the order of $10^{-13}/10^{-14}[m/g]$, extremely low values when compared with the typical sensitivity of detectors in use, which is in the order of picometers, $10^{-12}[m/g]$. This is certainly the greatest limitation of the Pasted design, which pays for its simplicity of modelling and construction with a limited working range in frequencies.

Parameter	Value
ρ_e	0.212
L	0.03 [m]
λ_b	1555 [nm]

Table 4.3: Parameters values

Furthermore, the effect of temperature, although neglected in the modelling of the sensor, has a very important effect within the measurement and is another downside of this architecture. But it is possible with a single solution to solve, or at least limit, the temperature effect and double the sensitivity of the device.

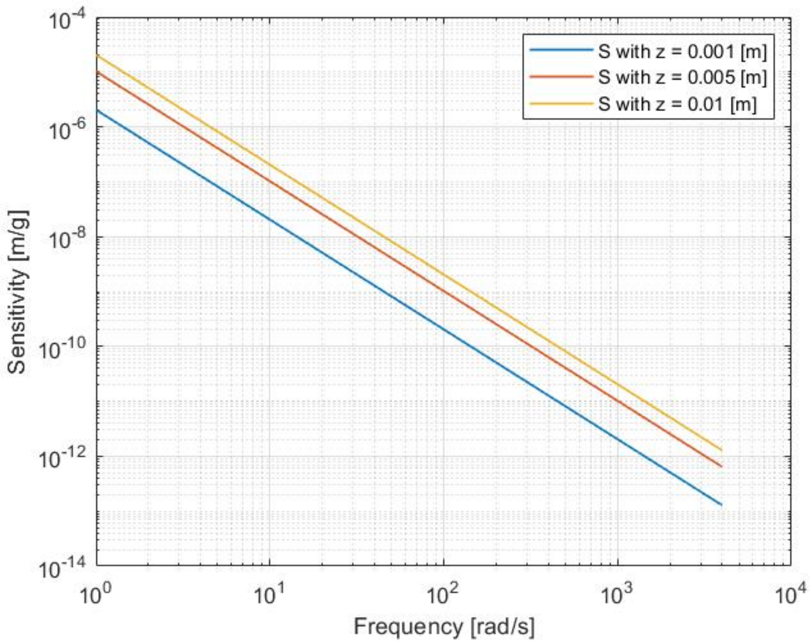

Figure 4.6: Log graph of Sensitivity vs Frequency

When the support flexes under the action of the inertial force, triggered by the vibration, it will be characterised by an opposed deformation on the outer surfaces, belly and back. While the former will be subject to compression, the second will be in traction and vice versa. Therefore, by using two FBGs, arranged symmetrically with respect to the neutral axis, it is possible to improve the characteristics of the sensor and limit the temperature effect. This can be demonstrated using the following formulae:

$$\begin{cases} \Delta\lambda_1 = \lambda_B[(1+p_e)\Delta\varepsilon + (\alpha_\Lambda + \alpha_n)\Delta T] \\ \Delta\lambda_2 = \lambda_B[-(1+p_e)\Delta\varepsilon + (\alpha_\Lambda + \alpha_n)\Delta T] \end{cases} . \tag{4.21}$$

By differentiating the two reflected wavelengths, the temperature-dependent term is eliminated and the sensitivity doubles as indicated by the multiplicative factor of the term concerning deformation:

$$\Delta\lambda_1 - \Delta\lambda_2 = 2\lambda_B(1+\rho_e)\Delta\varepsilon \tag{4.22}$$

In any case, it is important to remember that this formula is obtained through linearization and is therefore restricted within a certain working range, which is why the effect of temperature is not completely eliminated but limited.

4.4 Pasting Model

Bonding is one of the critical aspects of this design as the strain of the FBG will not be equal to that of the support surface. It is very convenient to introduce the Glue Transfer Factor, GTF, to estimate the losses due to the adhesive layer. This value, however, strongly depends on the glue line geometry and the type of material used. Several types of research [15] [16] have shown that the best strategy is to embed the fibre along the entire length of the support, this significantly improves the load transfer between the two elements. However, it is very difficult to obtain precise values under real conditions, the dimensions are extremely small and the bonding process is carried out manually, so it is almost impossible to respect tolerances in the [mm] range. For this reason, the evaluations made must absolutely take into account the real case and a testing phase is therefore indispensable to obtain a more accurate factor, possibly through a statistical investigation. As far as the substance to be used to achieve adhesion, epoxy resins are certainly the main candidate, as they possess excellent structural properties as well as being particularly suitable for bonding using plastics, which will be the main candidate for the sensor construction.

In general, the following indications for the best possible bonding can be obtained thanks to the research done by Wu et al [15]:

- The fibre should be bonded as close as possible to the axis of symmetry of the support.
- The longer the sensor length, the better the GTF.
- Excessive bonding thicknesses produce losses due to shear stress and reduce the transfer factor. In general, bonding thicknesses of 0.10-0.20 [mm] produce the best results, guaranteeing structural strength.
- The higher the elastic modulus of the adhesive, the lower the losses due to shear stress and the higher the transfer factor.

Considering these recommendations, a conservative GTF value may be in the range of 0.80-0.85. It is clear that the choice of glueing the fibre onto the support presents several challenges, but it was nevertheless preferred to the inscription of the FBG inside the structure for several reasons. First of all, this solution simplifies the design and manufacturing process of the part, also facilitating the pre-tensioning phase of the fibre itself. Furthermore, as shown by the paper [17] the thickness of the bonding, by increasing the distance of the FBG from the neutral axis of the support, can significantly improve the sensitivity of the sensor. This can be demonstrated by imposing the following assumptions:

- Each part remains in contact during the bending phase.
- The core and the fibre coating possess the same parameters.

Taking this into account, and assuming the diagram in figure (4.7), it is possible to change the value of z within equation (4.16). This makes it possible to consider the effect of the thickness of the bonding on the bending strain of the fibre:

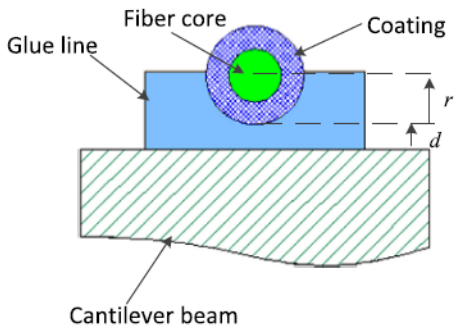

Figure 4.7: Model of beam,glue and FBG

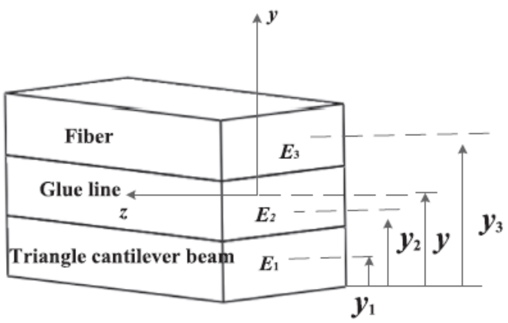

Figure 4.8: Structural Model considered

$$\varepsilon = \frac{3z}{\omega_0^2 L^2} a = 3 \frac{h/2 + d + r}{\omega_0^2 L^2} a \tag{4.23}$$

Where:

- d is the glue thickness;
- r is the coating radius of the FBG;
- h is the thickness of the support.

Substituting the new expression into equation (4.20) results in a new sensitivity value:

$$S_1 = (1 - \rho_e)\frac{3\alpha(h/2 + d + r)\lambda_B}{\omega_0^2 L^2} \tag{4.24}$$

Comparing this with the previous modelling, it is clear that the sensitivity is increased by a factor of η:

$$\eta = \frac{S_1}{S} = \frac{h/2 + d + r}{h/2} \tag{4.25}$$

Obviously this factor simply gives an indication that bonding can be exploited to improve the properties of the sensor, confirming one of the reasons for choosing this solution over the insertion of the fibre into the support material.

4.5 Support Dimensions and Mass

Once the mathematical description has been completed and the main characteristics governing the operation of this type of architecture are identified, it is now time to begin the support design phase. The main parameters on which to act are numerous, which is why the Matlab script in the appendix was used. The aim of the program is to simplify the performance calculation process as the main parameters of interest change. In this way, it is possible, as the material and geometric dimensions vary, to obtain the best characteristics in the form of natural frequencies and sensitivity. Some simplifications are made in this calculation phase:

- the effect of the bonding and the fibre on the dynamic and mass properties of the structure is not considered as it is negligible when compared to the size and weights of the support;
- again, the effect of structural damping for the calculation of eigenfrequencies is not taken into account, thus assimilating the whole assembly to a second-order mass-spring system;
- the beam hypothesis is considered valid.

In the first part of the script, one proceeds with the settings of the structural and optical parameters of interest. First and foremost, Young's modulus of the material used, on which the value of the support's eigenfrequencies depends. Next, the values concerning the properties of the optical fibre are defined, i.e. the strain optic coefficient and the wavelength of the propagated beam. At this stage, the parameter T, the minimum ratio between length and base width and between length and thickness, is also defined, thereby guaranteeing the validity of the beam hypothesis. This is because smaller values produce geometric shapes, similar to plates, which do not respect hypothesis (4) of the beam theory and this is very evident in the validation phase through the use of FEM analysis. The value of T=4.5 was obtained through various tests and validations, confirming itself as the minimum value to ensure the correspondence between the results of the Matlab script and those of the finite element analysis. Specifically, the value selected allows for a good correlation of the support's natural frequencies, a fundamental value in the evaluation of the validity of the device. Once this is done, vectors containing the possible beam lengths, possible base widths and possible thicknesses are defined, thus allowing the best combination capable of satisfying the desired characteristics to be investigated. At this point, three for-cycles are used, to obtain all possible combinations of dimensions, for the calculation of the flexural stiffness of the support. The formulae shown in section (4.2) are used here but with a novelty. As can be seen in figure (4.9), the equal strength architecture procures the shape of an isosceles triangle, thus with a vertex at the end. This, in addition to being very difficult to simulate with FEM, makes it almost impossible to position the mass at the end of the support. For this reason, the architecture under consideration cuts the triangle at 80% of its length to obtain a shape that is easier to implement.

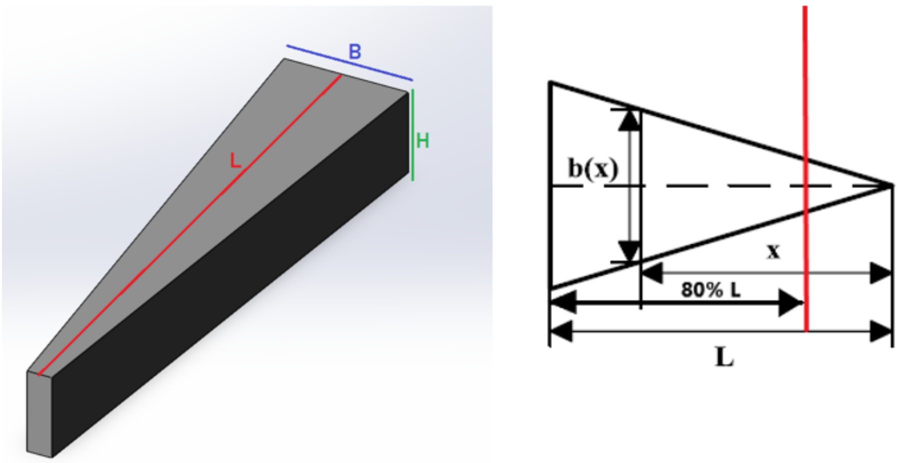

Figure 4.9: Geometry of the support

Having done this it is necessary to calculate the ratio between the length and the base width of the beam, this parameter is fundamental in the definition of the equal strength geometry, formula (4.7), and allows for the calculation of the value of width at the extreme end of the support, and thus eighty percent of the total length. This is necessary to extract the average width, as this geometry is characterised by a variable width and therefore variable cross-section, this makes the calculation of the inertia moment, which is necessary for the evaluation of the flexural rigidity, not straightforward. Using the values of width at the base and width at the extremity, it is possible to obtain an average measurement to be used for the calculation of the average moment of inertia. The latter finally allows the flexural rigidity of that specific combination of dimensions to be evaluated. Having done so, it is possible to estimate the value of the mass at the end of the beam to guarantee the desired dynamic properties. As also shown in the previous sections, the sensitivity of the pasted architecture is inversely proportional to the value of the support's own frequency. For this reason, the mass is calculated in such a way as to guarantee a maximum eigenfrequency in the order of 200 [Hz], using the formulae derived for mass-spring systems:

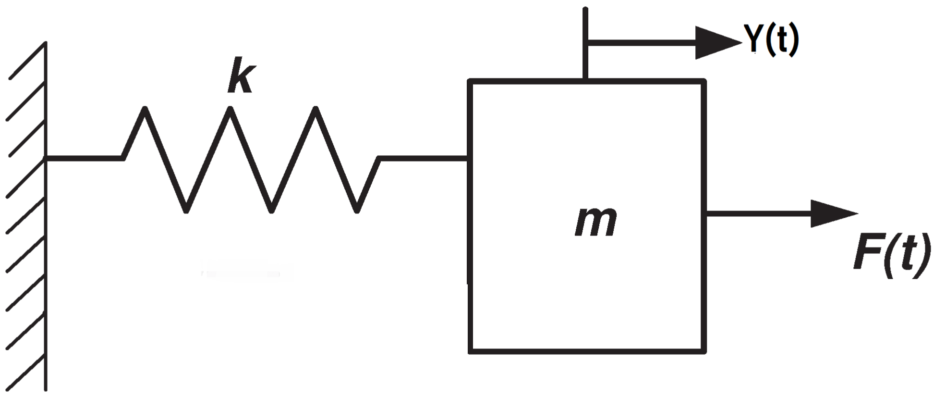

Figure 4.10: Mass and Spring system

$$m\ddot{Y} + K\dot{Y} = F \sin \omega t \tag{4.26}$$

Then the eigenfrequency is equal to :

$$\omega_0 = \sqrt{\frac{K}{m}} \tag{4.27}$$

then inversely, given the desired frequency and the stiffness obtained, the mass at the end of the beam can be calculated as:

$$m = \frac{K}{\omega_0^2} \tag{4.28}$$

In which the mass of the beam is neglected and the beam is assimilated to a spring with an elastic constant equal to the flexural stiffness of the structure. This can also be assessed by applying Rayleigh's method [18], which also considers the mass of the support and provides a more precise estimate of the frequency once the mass at the end has been determined:

$$m = W + \frac{33}{140} m_f \tag{4.29}$$

Where:

- W = weight of the lumped mass at the end of the beam;
- m_f = weight of the support.

This value can also be used as an alarm bell to detect discrepancies within the modelling and thus discard results that do not make sense to process. Specifically, when the frequency obtained via Rayleigh turns out to be very different from the frequency used for the mass calculation. This occurs mainly in one case, i.e. when the mass at the extremity has the same order of magnitude as that of the support, this invalidates the mass-spring modelling employed since in the calculation the latter is considered mass-less. For this reason, the acceptable solutions are those characterised by a lumped mass with a value of one or two orders of magnitude greater than that of the support.

3353x11 double

	1	2	3	4	5	6	7	8	9	10	11
57	369.1406	0.0300	0.0045	0.0015	2.1843e-04	0	9.0000e-04	1.2150e-04	3.3993e-04	1.1329e-12	194.5404
58	410.1563	0.0300	0.0050	0.0015	2.4270e-04	0	1.0000e-03	1.3500e-04	3.7770e-04	1.1329e-12	194.5404
59	486.1111	0.0300	0.0025	0.0020	2.8764e-04	0	5.0000e-04	9.0000e-05	3.7764e-04	1.5105e-12	199.6693
60	583.3333	0.0300	0.0030	0.0020	3.4517e-04	0	6.0000e-04	1.0800e-04	4.5317e-04	1.5105e-12	199.6693
61	680.5556	0.0300	0.0035	0.0020	4.0270e-04	0	7.0000e-04	1.2600e-04	5.2870e-04	1.5105e-12	199.6693
62	777.7778	0.0300	0.0040	0.0020	4.6022e-04	0	8.0000e-04	1.4400e-04	6.0422e-04	1.5105e-12	199.6693
63	875.0000	0.0300	0.0045	0.0020	5.1775e-04	0	9.0000e-04	1.6200e-04	6.7975e-04	1.5105e-12	199.6693
64	972.2222	0.0300	0.0050	0.0020	5.7528e-04	0	1.0000e-03	1.8000e-04	7.5528e-04	1.5105e-12	199.6693
65	1.1393e+03	0.0300	0.0030	0.0025	6.7416e-04	0	6.0000e-04	1.3500e-04	8.0916e-04	1.8882e-12	202.1847
66	1.3292e+03	0.0300	0.0035	0.0025	7.8651e-04	0	7.0000e-04	1.5750e-04	9.4401e-04	1.8882e-12	202.1847
67	1.5191e+03	0.0300	0.0040	0.0025	8.9887e-04	0	8.0000e-04	1.8000e-04	0.0011	1.8882e-12	202.1847
68	1.7090e+03	0.0300	0.0045	0.0025	0.0010	0	9.0000e-04	2.0250e-04	0.0012	1.8882e-12	202.1847
69	1.8989e+03	0.0300	0.0050	0.0025	0.0011	0	1.0000e-03	2.2500e-04	0.0013	1.8882e-12	202.1847
70	2.2969e+03	0.0300	0.0035	0.0030	0.0014	0	7.0000e-04	1.8900e-04	0.0015	2.2658e-12	203.5916
71	2625	0.0300	0.0040	0.0030	0.0016	0	8.0000e-04	2.1600e-04	0.0018	2.2658e-12	203.5916
72	2.9531e+03	0.0300	0.0045	0.0030	0.0017	0	9.0000e-04	2.4300e-04	0.0020	2.2658e-12	203.5916
73	3.2813e+03	0.0300	0.0050	0.0030	0.0019	0	1.0000e-03	2.7000e-04	0.0022	2.2658e-12	203.5916
74	4.1684e+03	0.0300	0.0040	0.0035	0.0025	0	8.0000e-04	2.5200e-04	0.0027	2.6434e-12	204.4542
75	4.6895e+03	0.0300	0.0045	0.0035	0.0028	0	9.0000e-04	2.8350e-04	0.0031	2.6434e-12	204.4542
76	5.2105e+03	0.0300	0.0050	0.0035	0.0031	0	1.0000e-03	3.1500e-04	0.0034	2.6434e-12	204.4542
77	7.0000e+03	0.0300	0.0045	0.0040	0.0041	0	9.0000e-04	3.2400e-04	0.0045	3.0211e-12	205.0200
78	7.7778e+03	0.0300	0.0050	0.0040	0.0046	0	1.0000e-03	3.6000e-04	0.0050	3.0211e-12	205.0200
79	1.1074e+04	0.0300	0.0050	0.0045	0.0066	0	1.0000e-03	4.0500e-04	0.0070	3.3987e-12	205.4106
80	22.9592	0.0350	0.0015	1.0000e-03	1.3585e-05	0	3.0000e-04	3.1500e-05	4.5085e-05	5.5489e-13	166.3727

Figure 4.11: Matlab script output example

Knowing now the value of the mass at the end of the support, one can proceed to calculate the main parameters of interest for evaluating the performance of the system. Three cascade for-cycles are again employed to obtain the values of each individual combination of size and associated mass. It is important at this stage to skim the results by discarding those characterised by dimensions that do not respect the T-ratio and cannot be treated as a beam. Compliant dimensions, on the other hand, are used to create a table showing the values of interest for each acceptable combination, in order:

1. flexural stiffness;
2. length of the untrimmed beam;
3. width at the base of the beam;
4. beam thickness;
5. mass at the extremity;
6. flags for compliance with imposed conditions;
7. width at beam end;
8. evaluation of the mass of the support obtained by multiplying the density of the material with the volume, calculated using the average width;
9. total mass, obtained by adding the previous with that at the end;
10. sensitivity of the sensor considering a GTF=1;
11. eigenfrequency value using the Rayleigh method.

Obviously, these values are not precise and are only an estimate due to the simplifications considered. They do, however, provide great help in understanding the trends of the quantities of interest as they vary in size, but, above all, they allow the FEM verification phase to start with an already defined and promising geometry.

Chapter 5

FEM Modelling and First Results

5.1 CAD and FEM Modelling

Using the data provided by the Matlab script, it is now possible to generate the geometry through the use of Solidworks. This software allows the creation of the CAD file subsequently exported in STEP AP 203 format for further verification through finite element analysis. This is a necessary step to confirm the accuracy of the mathematical modelling implemented in the script and for the confirmation of the assumptions used.

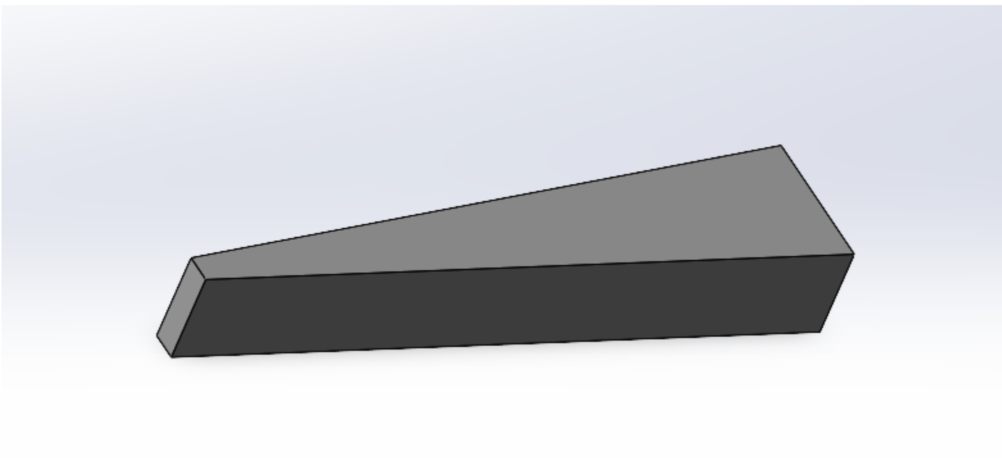

Figure 5.1: CAD model

In the verification procedure, the supports characterised by the best sensitivity and the practicability of realisation were analysed. All designs with extremely small dimensions or having one end with a width not capable of accommodating the lumped mass were excluded. Finite element analysis is carried out first to confirm the value of the support's natural frequencies and then to verify the deformation range of the surfaces. The software used is Hypermesh 2021 accompanied by the Optistruct solver. Each part was modelled through the use of HEXA-type solid elements, first using a 2-d mesh on one of the two surfaces and then extruding through the DRAG function the two-dimensional element. This produces a very regular three-dimensional mesh to which a PSOLID-type property is then associated. The support is subsequently constrained at the base by locking all six degrees of freedom of the corresponding nodes. Concerning the mass at the end of this first phase, this is simulated using CONM2 elements. These allow the concentration of a given mass on a single node, which is strategically positioned a few millimetres at the end of the support. The connection with the rest of the structure is ensured through the use of rigid elements of type RBE2. This simplification makes it possible to test the values obtained from the script very quickly and, if necessary, modify them if the eigenfrequency does not meet the requirements simply by varying the mass of the external node.

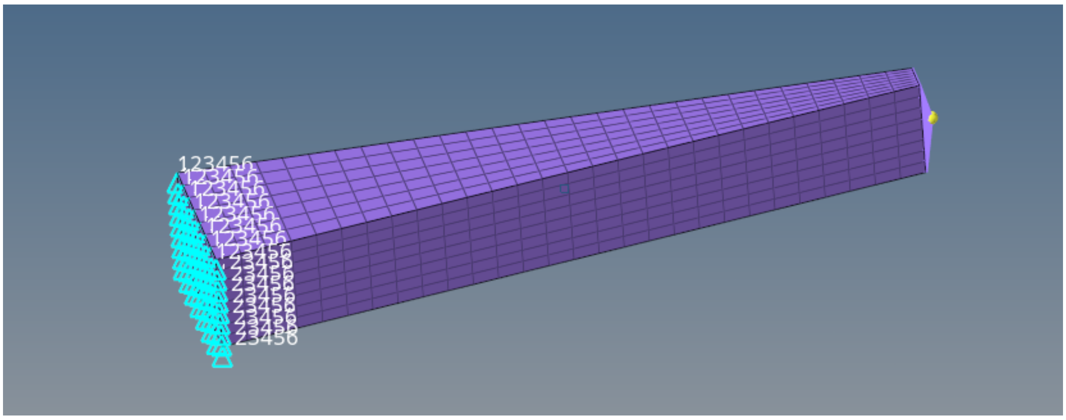

Figure 5.2: FEM model

Static analysis is conducted to visualise the compressive and tensile deformations, due to bending, by using a load step of type linear static. The results in figure (5.3) show a large area characterised by constant deformation thus confirming the effectiveness of the equal strength geometry. Obviously, the end is characterised by a small discontinuity, but this is not surprising, the beam theory, in fact, has extremely stringent validity assumptions that are far off from the real phenomenon. The result is therefore satisfactory, allowing the sensor to be bonded in a large area of the beam and mitigate the chirping phenomenon.

Instead, the modal analysis makes it possible to derive the natural frequencies of the support, which are fundamental values for defining the working range of the

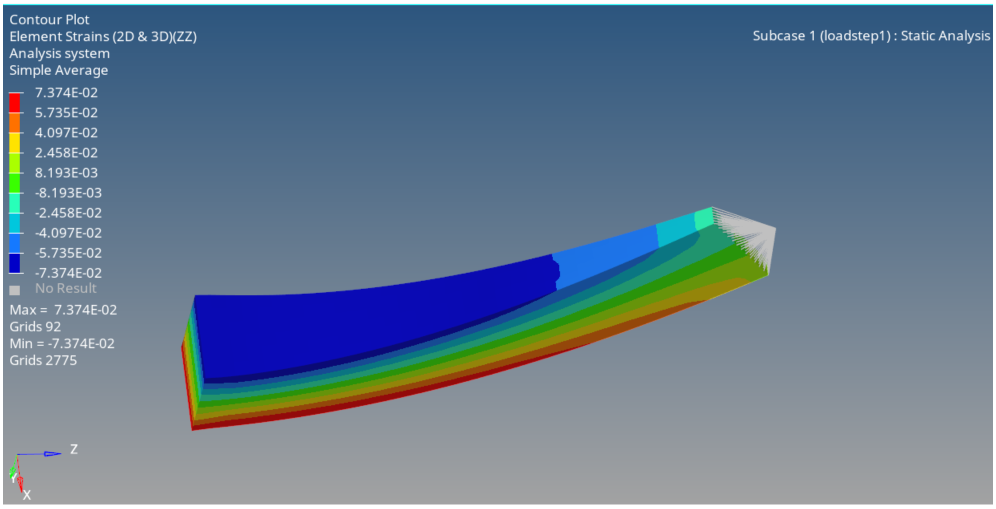

Figure 5.3: Static analysis results

sensor and for sensitivity calculations. It is obtained through the use of an EIGRL-type card that implements the Lanczos method for calculating the eigenvalues associated with the vibration modes. The equilibrium equation considered is as follows:

$$[K - \lambda M]x = 0 \tag{5.1}$$

In which;

- K is the component stiffness matrix;
- M is the mass matrix;
- λ the eigenvalue matrix.

In addition to defining the numerical value of the resonance frequencies, this operation allows the visualisation of the vibrational mode. In the case study, all those designs characterised by the first eigenfrequency in correspondence with the direction of the vibrational load are chosen. Therefore, the first vibration mode needs to be transverse to the cross-section of the supports. To ensure this, designs characterised by a thickness less than the width of the base of the support are selected. This is required to avoid, during testing, the occurrence of resonance at lower frequencies than desired or the combination of different vibrational modes in directions not compatible with the load.

5.2 Materials

The choice of material has a fundamental significance in the design process of the sensor, and specifically, the elastic modulus and the density have a primary influence in determining the support's natural frequency and its geometry. Furthermore, it must be remembered that the sensor must be easy to realise and, consequently, the use of commonly used materials is preferred. The script allowed an immediate evaluation of the possible designs when varying the material used. It is clear that, as the elastic modulus increases, with the same eigenfrequency and sensitivity, the overall size of the support decreases while the weight of the mass at the extreme increases. This is easily understood from formulae (4.10) and (4.28), a high Young's modulus results in a higher flexural stiffness for the same size and consequently, it will be necessary to use masses of greater weight to obtain the same eigenfrequencies. Although this may seem an advantage, it does not actually take into account the geometry of the mass to be placed at the extreme, which in some cases, even when using dense materials such as lead, turns out to have geometric dimensions comparable with those of the specimen itself. Consequently, two materials, aluminium and PLA, were selected for the evaluation of the support. Both are modelled within the fem analysis through the MAT1 card and therefore considered isotropic and without structural damping.

Material	Young Modulus [GPa]	Density [Kg/m^3]	Poisson Ratio
Aluminium	70	2700	0.3
PLA	3.5	1250	0.3

Table 5.1: Material properties

To prove the former statement, two supports with the same dimensions but different materials are compared:

Material	K [N/m]	L [m]	B [m]	h [m]	m [Kg]	ω [Hz]	S [m/g]
All.	1.9e4	0.01	0.0015	0.001	0.0116	206.86	1.35e-11
PLA	9.8e3	0.01	0.0015	0.001	0.00058	206.52	1.35e-11

Table 5.2: Comparison of PLA and Aluminium

There is an order of magnitude of difference between the two masses, which makes it inconvenient and in some cases even impossible to construct the aluminium support. Although there is the possibility of finding an acceptable and practically viable combination of sizes and mass, the solution has a much lower sensitivity than its plastic counterpart. The latter is therefore chosen as the material for the construction of the support and will henceforth characterise the results and simulations shown.

5.3 Dynamic Response

A frequency response analysis is conducted to visualise the response of the support under the action of a harmonic load. The resulting bode graph allows the evaluation of the dynamic response of the structure and also serves to confirm the validity of the mathematical model.

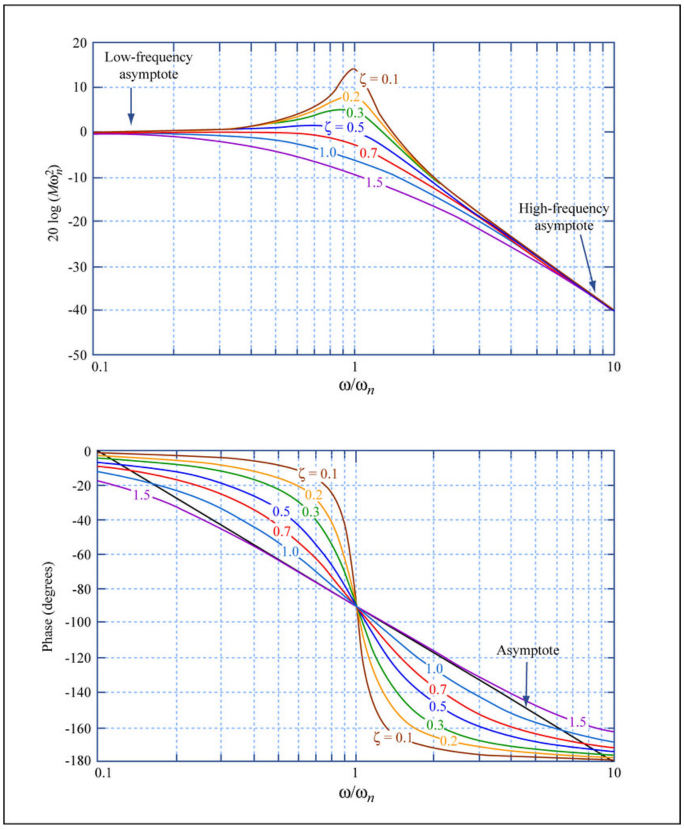

Figure 5.4: Bode plot of a second order system

The objective is to obtain a bode typical of a second-order system, figure (5.4), which would confirm the assumptions made in the previous chapters. The algorithm used within Hypermesh is the Direct Frequency Response Analysis, the equation that is solved is as follows:

$$M\ddot{u} + C\dot{u} + Ku = fe^{i\Omega t} \tag{5.2}$$

In which;

- K is the stiffness matrix;
- M is the mass matrix;
- C is the damping matrix;
- u is the displacement vector;
- f is the load vector;
- Ω is the angular frequency at which the load is applied.

The damping coefficient is assumed to be constant as well as uniform and introduced within the simulation through the use of the GE coefficient within the material tab. This however only provides an estimate and represents a simplification. A more precise value requires experimental evaluations once the support has been constructed. The frequency-dependent dynamic load is defined through the use of the RLOAD card, which allows the introduction of a harmonic load with variable frequency. In this case, it was decided to consider the entire structure, and therefore each node, subjected to the action of an acceleration of module 1 $[m/s^2]$.

5.4 First Results

Through the use of the script, it was possible to identify an ideal combination of measures, capable to guarantee the frequency constraint, characterised by good sensitivity and, above all, having a mass with dimensions compatible with the rest of the support. The main characteristics and the results obtained through FEM, carried out according to the above indications, are shown in the table below:

L [m]	B [m]	h [m]	m [Kg]	ω [Hz]	S [m/g]
0.028	0.006	0.004	0.005	232.5	4.4e-12

Table 5.3: Characteristics of the studied support

The dynamic analysis was conducted with a damping coefficient of 0.005. The image below shows the bode of one of the nodes on the free end of the support. The behaviour is that of a typical second-order system, characterised by the phenomenon of resonance in the presence of the first eigenfrequency and a phase delay of approximately 180 degrees at high frequencies. This is a further confirmation of the correct modelling of the phenomenon and allows, as shown in the next chapter, the optimisation of the design and the creation of a structure capable of being tested in the laboratory.

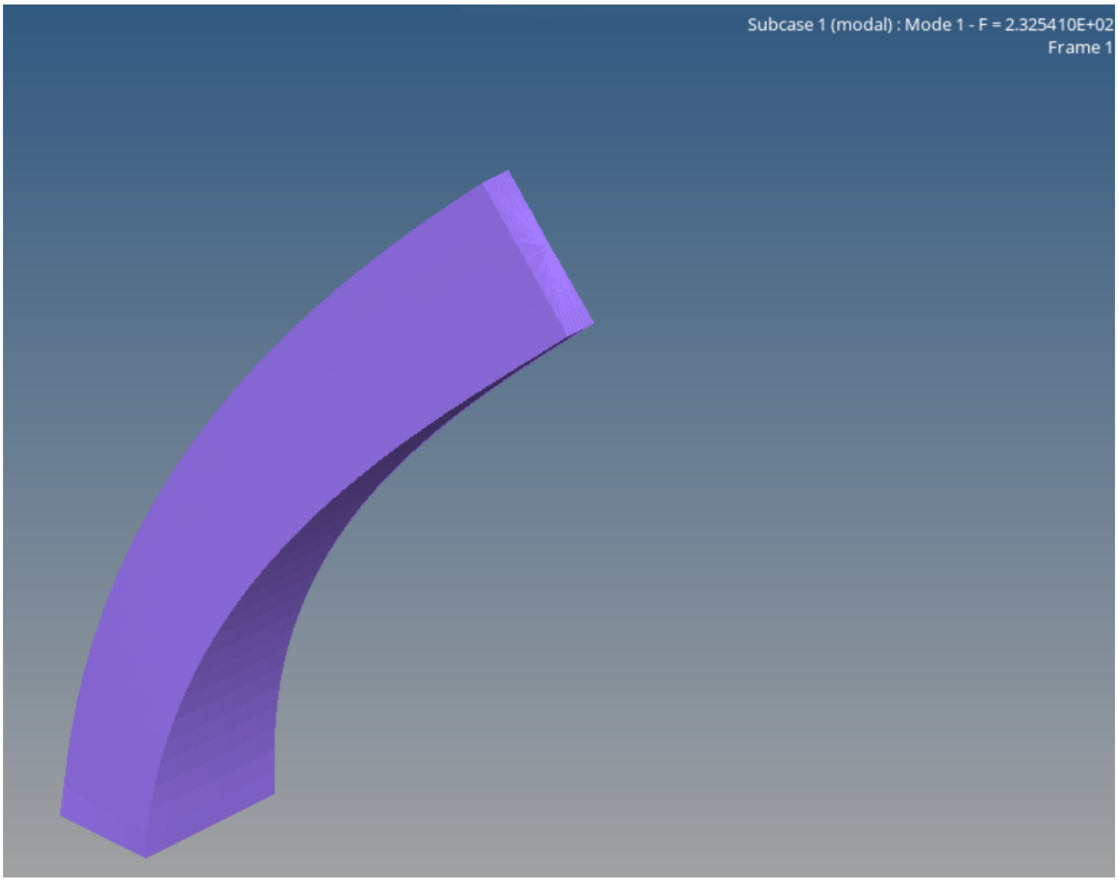

Figure 5.5: Modal analysis results

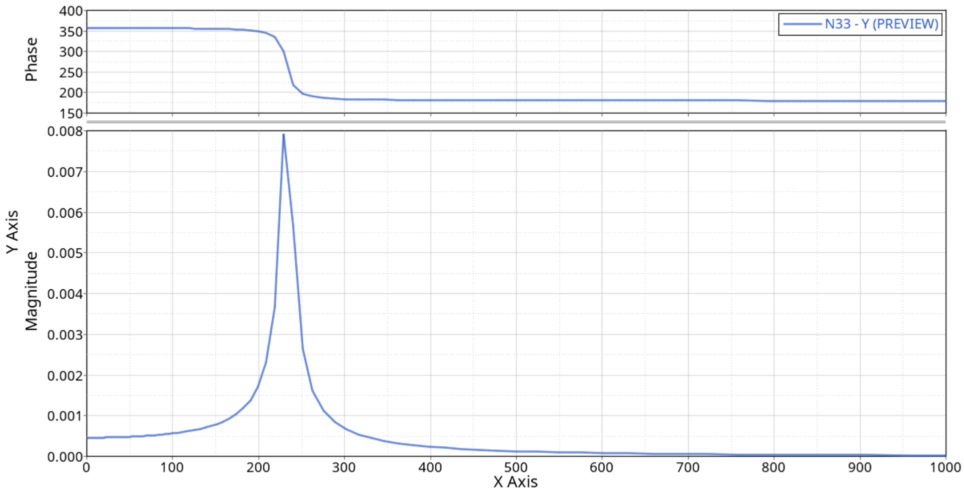

Figure 5.6: Dynamic analysis results

Chapter 6

Testing Sets and Final Results

6.1 Support Optimization and Mass Implementation

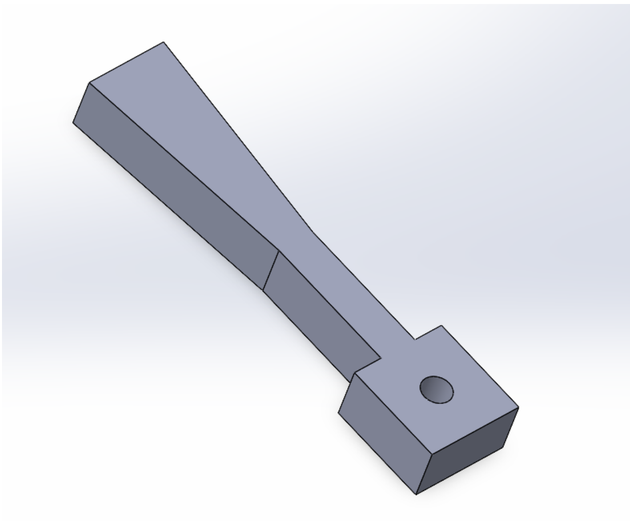

Figure 6.1: CAD model of the optimized support

The geometry of the prototype, although functional, makes its practical implementation very difficult. The free end is less than a millimetre in size, which makes it difficult and sometimes impossible to insert the external mass. To avoid this, the script in the appendix is modified, this time considering the entire length and not the remaining 80%. In addition, the equal strength geometry is used along a smaller section, i.e. that intended for bonding the fibre. The remaining portion has a constant, rectangular shape, which ends with a special section intended for housing the mass. As can be seen from the photo (6.2), the structural properties of the equal strength are preserved while there are some differences in the values of the eigenfrequencies. To remedy this, the thickness of the beam and the value of the mass at the end are modified. The latter plays a fundamental role in determining the resonance frequency of the specimen and therefore requires special attention. The housing is characterised by a rectangular section with a central hole with a radius of 1 [mm]. Inside of which passes an iron wire to be fitted with lead balls, photo (6.3). These are all simply procurable materials and, above all, provide enormous flexibility. In fact, for the testing phase, it is planned to produce the sensor through 3D printers, a process known to be characterised by geometric imperfections, voids and therefore non-constant density and anisotropy of structural properties. This will most likely result in discrepancies between the simulated and actual frequency values.

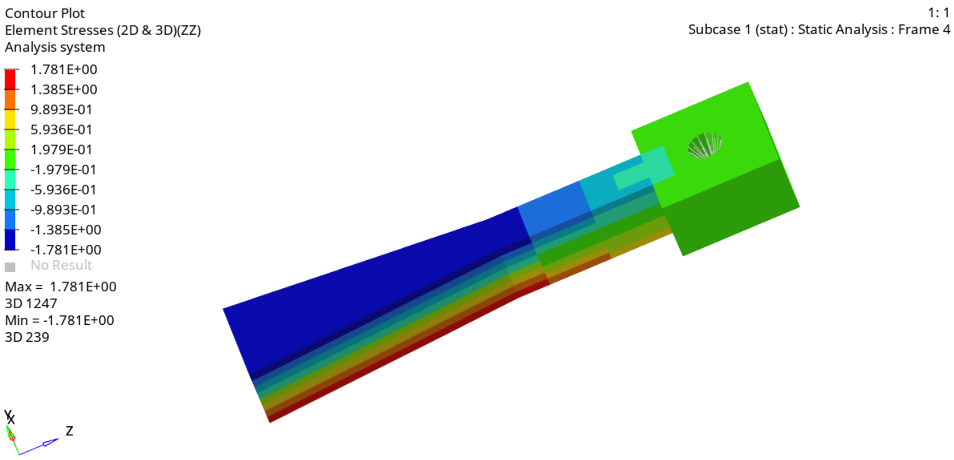

Figure 6.2: Stress distribution of the optimized support

To overcome this, the design used makes it very easy to replace the lead spheres with different masses to achieve the desired dynamic properties. The arrangement is symmetrical with respect to the neutral axis of the test specimen and the position is ensured through the use of the wire passing through the hole. The FEM modelling involves the use of a CONM2 element positioned in the centre of the hole and connected to the rest of the nodes through the use of the RIGID RBE2 elements.

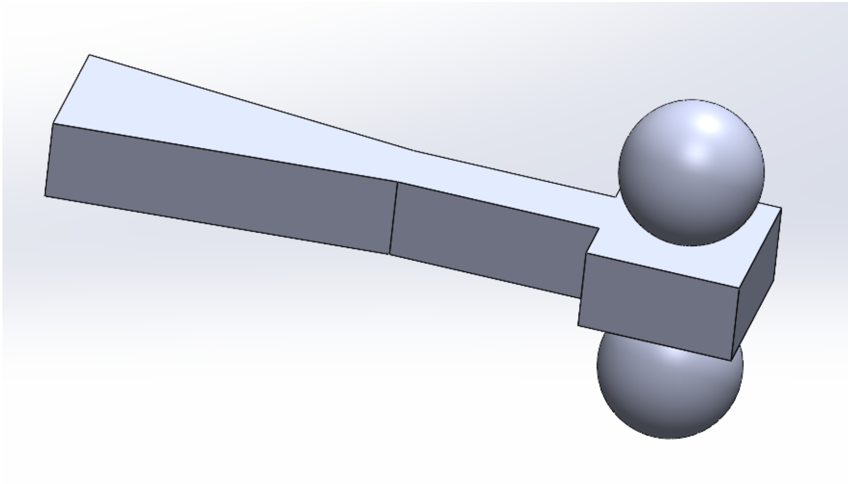

Figure 6.3: CAD model with two mass of two grams

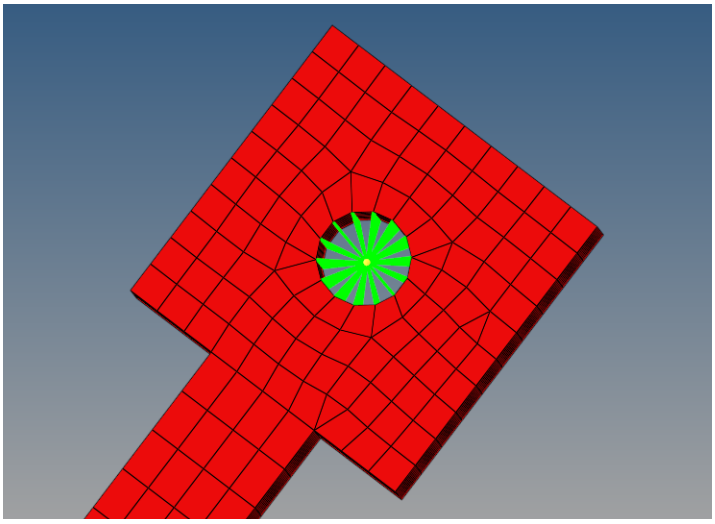

Figure 6.4: FEM modelling of the external mass

6.2 Test Setting

At this point, the methodology and the devices for the experimental verification of the design must be defined. The production of the vibration is achieved through the use of a mechanical shaker capable of generating the linear oscillatory motion in the direction of interest. This is accompanied by two devices:

- Function Generator: which allows the solicitation signal to be generated in terms of both shape and frequency.

- Amplifier: which allows setting of the gain, the amplitude of the load, and a current limit.

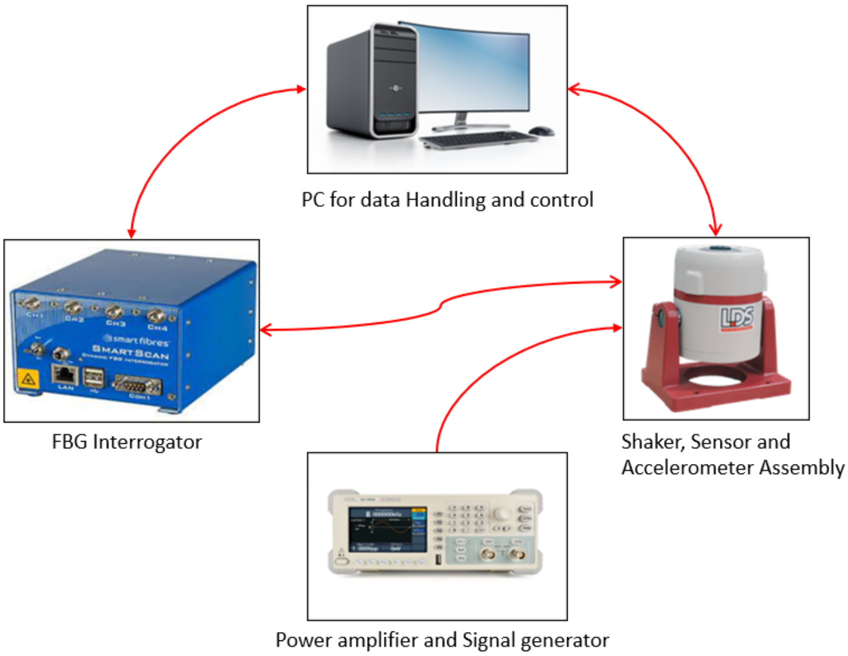

Figure 6.5: Test setting and devices

The optical signal, on the other hand, is generated and acquired by the interrogator, which has a dedicated channel for each sensor and is managed via the SmartSoft software. The device is powered by a power unit and has the following features:

Wavelength range	40 [nm] (1528-1568 [nm])
N° of optical channel	4
Maximum scan frequency	25 [KHz]
Repeatability	< 1 [pm]
Dynamic range	37 [dB]
Dimensions	140x115x85 [mm]
Weight	0.9 [Kg]

Table 6.1: SmartScan FBG Interrogator data sheet

The scheme of the entire apparatus should follow the figure (6.5). The objective is to first verify the support's own frequency values and then to check the actual output of the fibre with the acceleration value to which it is subjected. To do this, however, one must first create the physical sensor carrier. This consists of three parts that are connected together using four threaded pins with nuts and washers. The aim is to ensure the structural integrity of the entire assembly during stress and the attainment of its own frequencies at higher values than those of the support. The three components are defined as follows:

1. Upper Shell.
2. Middle Shell.
3. Lower Shell.

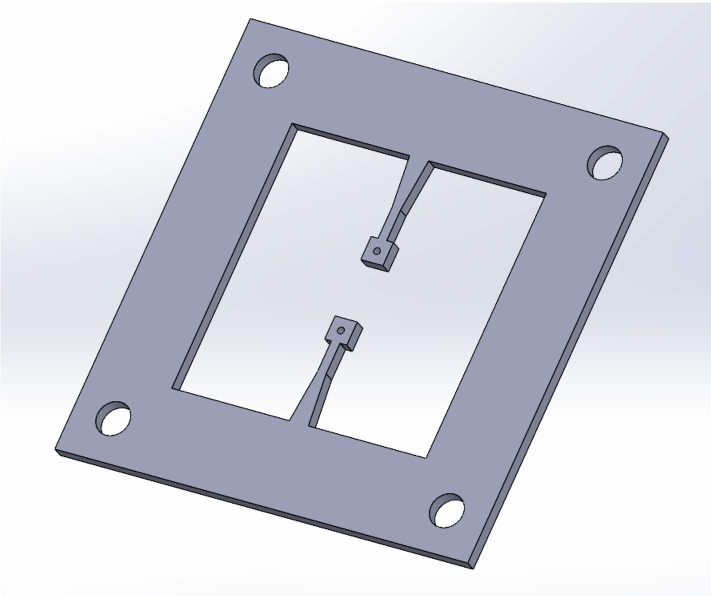

Figure 6.6: Middle Shell CAD model

The fundamental component, namely the one featuring the support and in which the FBG is positioned, is the middle shell. The geometry of this is designed to simplify printing operations, without the use of a carrier and is always secured to the printing bed. As can be seen, the use of two supports is planned, this is to ensure dynamic stability during solicitation and provide the possibility of multiple readings with different bonding and mass parameters.

The top part or upper shell acts mainly as a casing and is characterised by an internal space that ensures free flexural movement of the support. A hole of a radius of 4 [mm] and a depth of 12 [mm] is inserted as a housing for the mounting

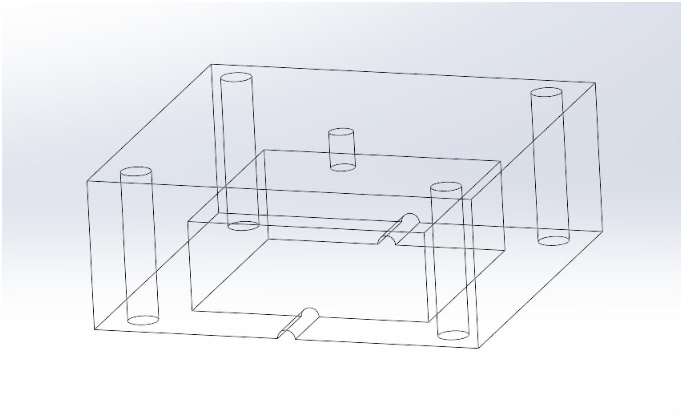

Figure 6.7: Top Shell inside view

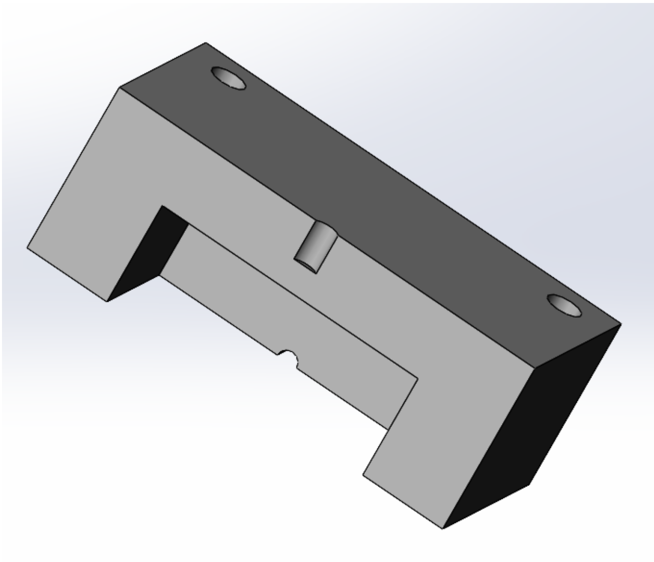

Figure 6.8: Top Shell section view

of an accelerometer. This is required to compare the acceleration value measured by the optical device. The lower shell, or lower part, allows the attachment of the assembly to the mechanical shaker through the hole of radius 7 [mm]. Four holes, both in the upper and lower shell, of radius 3 [mm] are provided for the passage of the fibres, as in the figure (6.9).

The verification of the eigenfrequencies is again obtained through FEM analysis. In this case, the middle shell is first studied by constraining the entire surface but excluding the sections of the support and those affected by the passage of the holes. The frequencies obtained tend to be slightly lower than those obtained considering

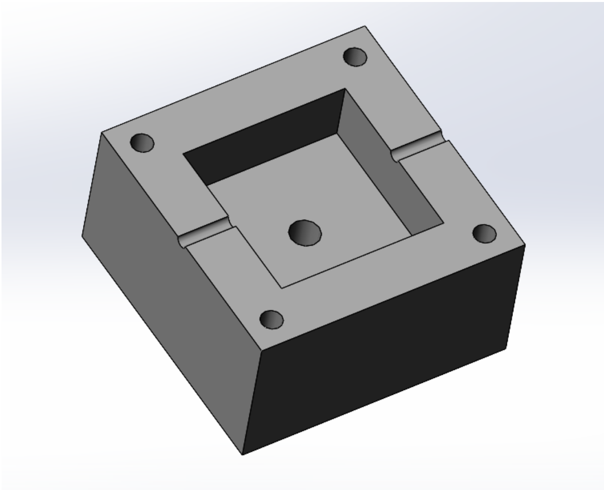

Figure 6.9: Bottom Shell CAD model

the isolated support due to the back flap increasing the effective length of the beam. In any case, thanks to the flexibility of the design, it is sufficient to modify the value of the masses at the end to achieve the desired result. Once this has been verified, the assembly is studied as a single piece, making an equivalence of the nodes in common with the middle-lower and upper shell. This is obviously a simplification, but it gives a good idea of the values of the eigenfrequencies involved. The whole is constrained on all 6 degrees of freedom by a node within the hole of the lower shell. In addition, the result is confirmed by separately studying the three pieces connecting the nodes related to the four fastening holes to their central node via rigid elements of type RBE2.

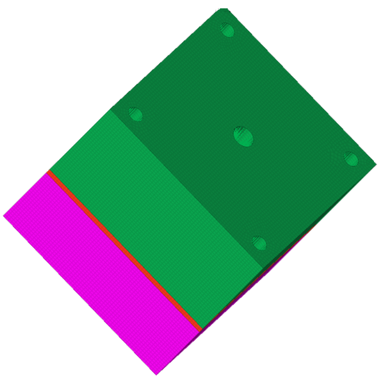

Figure 6.10: Full Sensor mesh model

6.3 Final Results

In this final section, the details of the geometries and the main results of the constituent component of the final assembly are laid out. First of all, the measurements of the isolated support and the results of the modal analysis are shown.

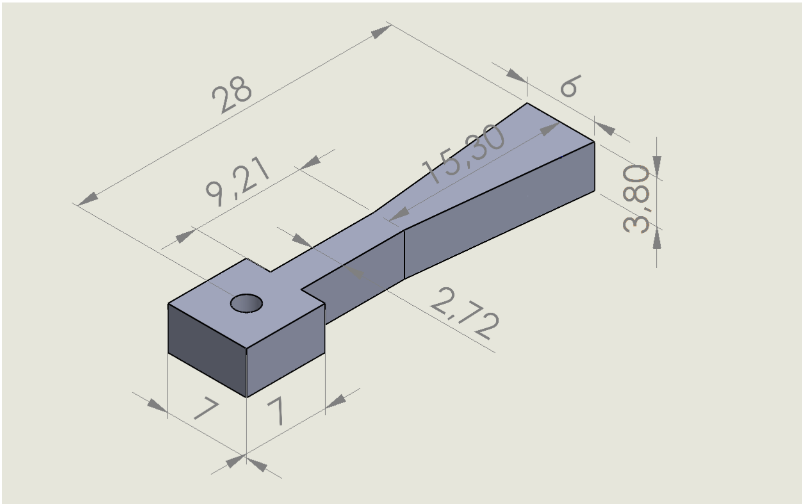

Figure 6.11: Final support dimensions in [mm]

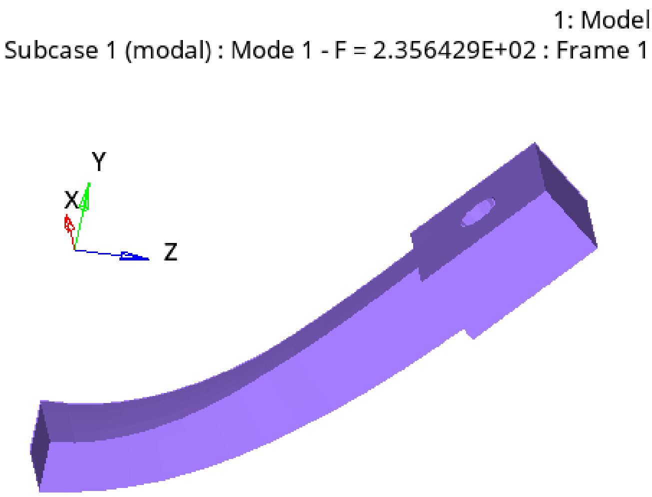

Figure 6.12: Final modal analysis results

The frequency achieved is higher than the 200 [Hz] desired to take into account the increase in the effective length of the support once the assembly has been analysed with the Middle Shell.

External Mass [Kg]	First Frequency
0.004	235.64 [Hz]

Table 6.2: Modal analysis mass and results

The support is then connected together with the middle shell as defined in the previous section. This, for the reasons already stated, has the same thickness as the beam and the resulting modal analysis takes into account the presence of the holes for the passage of the fibres, figure (6.14). The value of the external mass used remains the same as in the previous case.

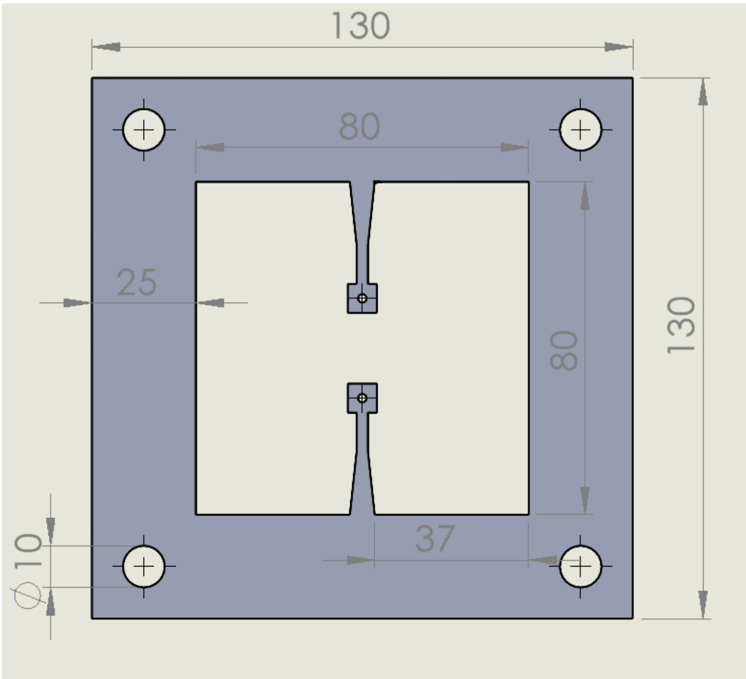

Figure 6.13: Middle Shell dimensions in [mm]

Total Mass [Kg]	First Frequency
0.059	212.33 [Hz]

Table 6.3: Middle Shell total mass and frequency

Lower and upper shells are manufactured separately, the interface section has the

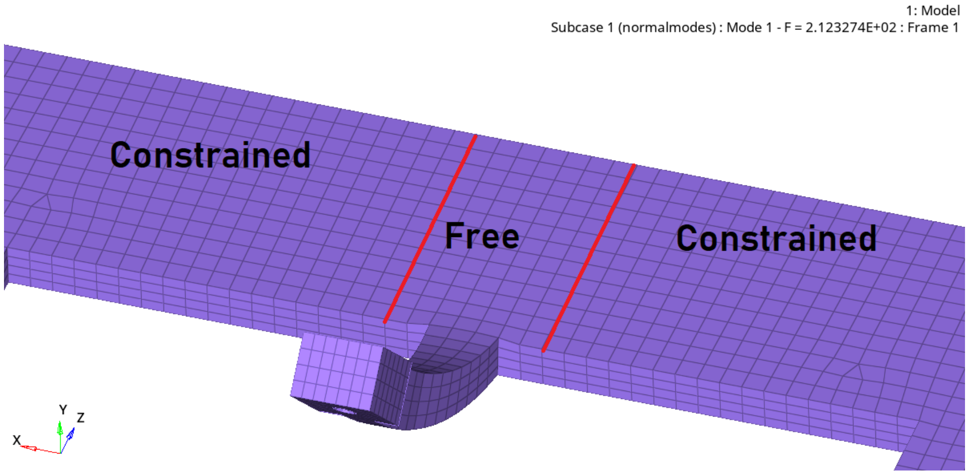

Figure 6.14: Middle Shell modal analysis results

same dimensions as the middle shell's flap with coinciding holes for mounting. The internal vacuum that is created once all three components are assembled ensures the free movement of the support during the vibration.

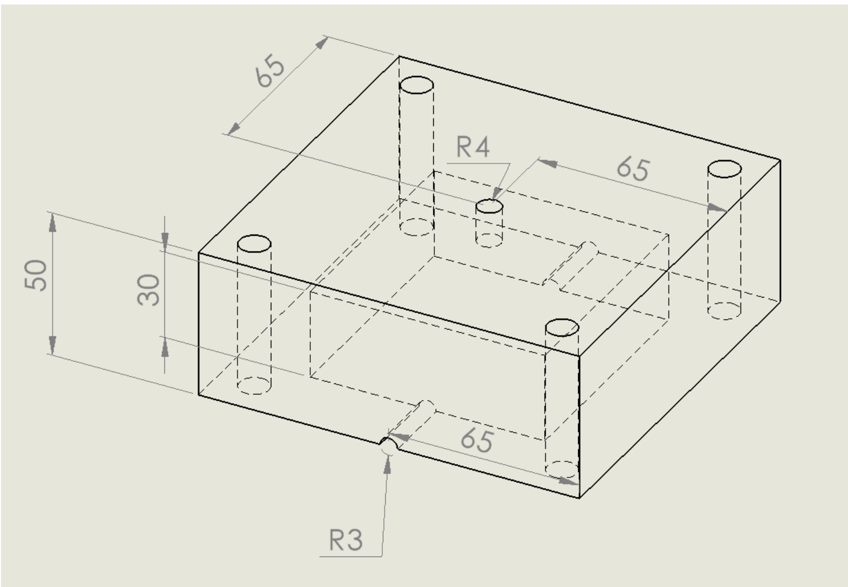

Figure 6.15: Upper Shell dimensions in [mm]

The external masses, on the other hand, are made of lead, thus considering a density of 11000 $[Kg/m^3]$ and possess a spherical shape. To obtain a total mass of 4 [g] per support two spheres of radius equal to 0.0035 [mm] are used. For this

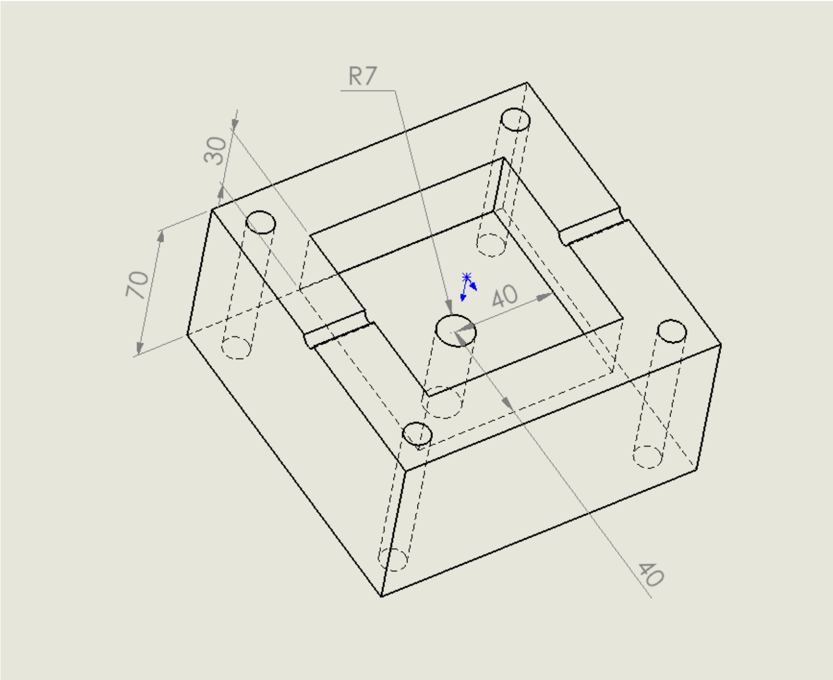

Figure 6.16: Lower Shell modal dimensions in [mm]

purpose, common fishing sinkers can be used if welded to the iron wire passing through the hole at the end of the support.

Figure 6.17: Typical lead sink

Concerning the dynamic study of the assembly, the results indicate values of frequencies relating to the normal modes of the total device greater than those of the beam. This makes it possible to ensure correct vibration detection during the testing phase by avoiding the occurrence of combined modes. The table shows the frequencies for the complete assembly, starting with the fifth normal mode, which affects the entire structure and not just the cantilever beam. It is important to emphasise that the first modes affecting the entire structure in the direction of load are the eighth and ninth.

N° normal mode	Frequency [Hz]
5	357.13 [Hz]
6	405.13 [Hz]
7	406.08 [Hz]
8	1075.63 [Hz]
9	1830.20 [Hz]

Table 6.4: Normal mode frequencies of the assemblies

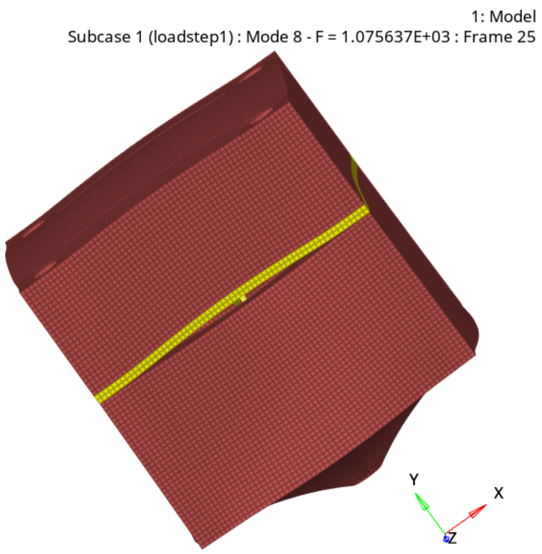

Figure 6.18: Normal mode in the direction of the load

Finally, the sensitivity of the sensor can be estimated using the formula (4.20) and by making the below conservative considerations:

1. Using the value of the eigenfrequency obtained in the Middle Shell analysis.
2. Considering an effective beam length range from the centre of the hole to beyond the base of the beam to the flap section of the middle shell.
3. Using a glue transfer factor of 0.85 and neglecting the glue thickness.
4. Multiplying the obtained sensitivity by two as two FBGs are used per support.

Beam length range [mm]	Sensitivity [pm/g]
[28-32]	[8.30-6.36]

Table 6.5: Sensitivity range of the sensor

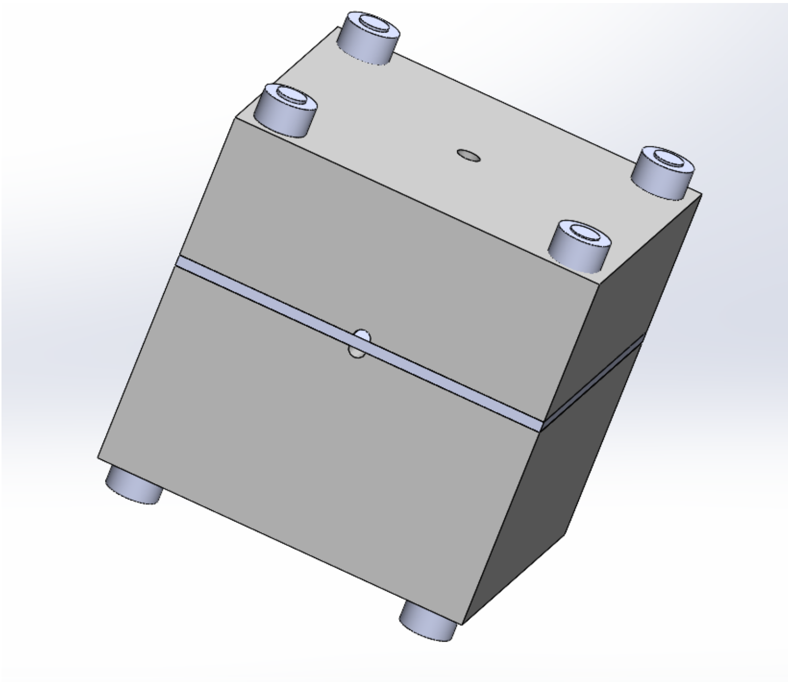

Figure 6.19: Complete assembly with fasteners

Whereas if one considers the minimum shift in wavelength detected by the interrogator, typically $\Delta\lambda_B$ is in the order of 0.1 [pm], through the formula (6.2) one can derive the overall minimum change in acceleration perceived by the instrument:

$$S = \frac{\Delta\lambda_B}{a} = [8.30 - 6.36][pm/g] \tag{6.1}$$

$$a_{min} = \frac{\Delta\lambda_B}{S} = \frac{0.1}{[8.30 - 6.36]} = [0.012 - 0.015][m/s^2] \tag{6.2}$$

Chapter 7

Conclusion and Future Works

The aim of this thesis is to outline the main characteristics of vibration detection sensors using FBG technology. The physical phenomenon and main attribute of these particular optical fibres are explained. The main designs within the scientific literature are indicated, outlining the pros and cons of each. Subsequently, the procedure of designing a possible sensor is shown, taking into account the restrictions caused by the practical realisation of the instrument. Step by step the assumptions are justified and the mathematical modelling implemented is verified through the use of finite element analysis. In addition, a simple Matlab script is created and made available capable of identifying the best geometries and materials for the realisation of a support for the Pasted architecture. Finally, the testing procedure, useful for validating the implemented modelling, is outlined. The essential tools for the correct execution of the activity are shown and some expected results are calculated. To enable this, the design of a casing structure for the support is carried out with particular attention to its dynamic properties to avoid the occurrence of resonance at frequencies lower than the beam's natural one. Unfortunately, it was not possible to carry out the latter due to logistical problems, but in any case, all the elements are available to carry it out in the short term. The next steps in the development obviously require the collection and verification of data from the mechanical shaker tests. An important improvement is certainly a better characterisation of the structural properties of the material used for the construction of the sensor and a study of the effects of bonding on the main properties of the device. Once this has been done, one can think about improving the architecture to minimise the weight, and size and improve the performance for the operational application of the technology. This has all the credentials for widespread use in certain sectors but the challenges it presents are still very difficult to overcome, especially when considering the footprint, cost and performance of interrogators. It is therefore essential to persevere with research in this field to obtain a feasible solution in the near future featuring lower weights, the ability of distributed measurements, high performance and immunity to electromagnetic interference.

Appendix A

Matlab Script

```
clc
clear all
%IMPOSTAZIONE DEI PARAMETRI STRUTTURALI%
E = 3.5; %modulo di Young in N/m^2 = Pascal
T = 4.5; %rapporto L/B minimo per avere ipotesi di trave
rhoe = 0.212; %coefficiente strain optic
rho = 1250; %densità del materiale in Kg/m^3
lambdam = 1.555e-06; %[m]
%IMPOSTAZIONE DEI PARAMETRI GEOMETRICI%
L = (0.01:0.005:0.10); %lunghezza totale della trave [m]
B = (0.001:0.0005:0.1);%larghezza all'incastro della base [m]
h = (0.001:0.0005:0.01); %spessore della trave, costante [m]
%CALCOLO RIGIDEZZE FLESSIONALI%
for i=1:length(L)
   c = L(i)-80/100*L(i);
     for j=1:length(B)
         rapporto = L(i)/B(j);
         bestremo = c/rapporto;
         bmedio = (B(j)+bestremo)/2;
            for n=1:length(h)
                 Imedio = (bmedio*h(n)^3)/12;
                 K =  (3*E*Imedio)./(0.8*L(i)^3);
                 Kris(i,j,n) = K;
            end
      end
end
%CALCOLO MASSA ALL'ESTREMITA'%
m = Kris./(1300^2);    %%209 hz
Tabella = zeros(numel(Kris),11);
contatore = 1;
%CALCOLO PRESTAZIONI
```

```
for v = 1:length(L)
    for u = 1:length(h)
        for w = 1:length(B)
         if ((80/100*L(v)/h(u) >= T) && (80/100*L(v)/B(w) >=T) && (h(u)<=0.9*B(w)))
            Tabella(contatore,6) = 0;
            Tabella(contatore,1) = Kris(v,w,u);
            Tabella(contatore,2) = L(v);
            Tabella(contatore,3) = B(w);
            Tabella(contatore,4) = h(u);
            Tabella(contatore,5) = m(v,w,u);
            c = L(v)-80/100*L(v);
            rapporto = L(v)/B(w);
            bestremo = c/rapporto;
            bmedio = (B(w)+bestremo)/2;
            Tabella(contatore,7) = bestremo;
            Tabella(contatore,8) = 0.8*L(v)*bmedio*h(u)*rho;
            Tabella(contatore,9) = Tabella(contatore,8) + Tabella(contatore,5);
            Tabella(contatore,10) = (1-rhoe)*((3*(h(u)/2)*lambdam)/((Kris(v,w,u)/m(v,w,u))*80/100*L(v)^2));
            Tabella(contatore,11) = (sqrt(Tabella(contatore,1)/(Tabella(contatore,8)*(33/140)+Tabella(contatore,5))))/(2*pi);
            contatore=contatore+1;
         else
            Tabella(contatore,6) = 1;
            Tabella(contatore,1) = Kris(v,w,u);
            Tabella(contatore,2) = L(v);
            Tabella(contatore,3) = B(w);
            Tabella(contatore,4) = h(u);
            Tabella(contatore,5) = m(v,w,u);
            contatore=contatore+1;
         end

        end
    end
end
conto = 1;
%Generazione tabella "pulita" scartando i valori
%che violano le ipotesi
for str =1:numel(Kris)
    if ((Tabella(str,6) ~= 1) && (Tabella(str,11)>180))
    Tabellapulita(conto,:) = Tabella(str,:);
    conto = conto+1;
    end
end

[M,indice ]=max(Tabellapulita(:,10))
```

Bibliography

[1] Grand View Research. «Fiber Optics Market Size, Share & Trends Analysis Report By Type (Single Mode, Multimode, Plastic Optical Fiber), By Application (Telecom, Military & Aerospace, Medical), And Segment Forecasts, 2019 - 2025». In: (2019) (cit. on p. 6).

[2] Alireza Behbahani, Mehrdad Pakmehr, and William A Stange. «Optical Communications and Sensing for Avionics». In: *Springer Handbook of Optical Networks*. Springer, 2020, pp. 1125–1150 (cit. on p. 18).

[3] Tianliang Li, Jinxiu Guo, Yuegang Tan, and Zude Zhou. «Recent advances and tendency in fiber Bragg grating-based vibration sensor: A review». In: *IEEE Sensors Journal* 20.20 (2020), pp. 12074–12087 (cit. on p. 21).

[4] Guang Chen, Keqin Ding, Qibo Feng, Xinran Yin, and Fangxiong Tang. «Strain transfer mechanism of grating ends fiber Bragg grating for structural health monitoring». In: *Structural Durability & Health Monitoring* 13.3 (2019), p. 289 (cit. on p. 22).

[5] Liang Fang, Tao Chen, Ruiya Li, and Shihua Liu. «Application of embedded fiber Bragg grating (FBG) sensors in monitoring health to 3D printing structures». In: *IEEE Sensors Journal* 16.17 (2016), pp. 6604–6610 (cit. on p. 22).

[6] Tianliang Li, Yuegang Tan, Yi Liu, Yongzhi Qu, Mingyao Liu, and Zude Zhou. «A fiber Bragg grating sensing based triaxial vibration sensor». In: *Sensors* 15.9 (2015), pp. 24214–24229 (cit. on p. 22).

[7] Dakuan Yu, Xueguang Qiao, Xiangyu Wang, and Jianlin Zhao. «Study on a fiber Bragg grating accelerometer based on push-pull compliant cylinders». In: *Eleventh International Conference on Information Optics and Photonics (CIOP 2019)*. Vol. 11209. SPIE. 2019, pp. 547–555 (cit. on p. 22).

[8] Kuo Li, Tommy HT Chan, Man Hong Yau, David P Thambiratnam, and Hwa Yaw Tam. «Experimental verification of the modified spring-mass theory of fiber Bragg grating accelerometers using transverse forces». In: *Applied Optics* 53.6 (2014), pp. 1200–1211 (cit. on p. 22).

[9] Tianliang Li, Chaoyang Shi, Yuegang Tan, Ruiya Li, Zude Zhou, and Hongliang Ren. «A diaphragm type fiber Bragg grating vibration sensor based on transverse property of optical fiber with temperature compensation». In: *IEEE Sensors Journal* 17.4 (2016), pp. 1021–1029 (cit. on p. 22).

[10] Byoungho Lee. «Review of the present status of optical fiber sensors». In: *Optical fiber technology* 9.2 (2003), pp. 57–79 (cit. on p. 25).

[11] Yong Zhao and Yanbiao Liao. «Discrimination methods and demodulation techniques for fiber Bragg grating sensors». In: *Optics and Lasers in Engineering* 41.1 (2004), pp. 1–18 (cit. on p. 25).

[12] Jinjie Chen, Bo Liu, and Hao Zhang. «Review of fiber Bragg grating sensor technology». In: *Frontiers of Optoelectronics in China* 4.2 (2011), pp. 204–212 (cit. on p. 25).

[13] Li Xiong, Yongxing Guo, Wanhuan Zhou, Min Chen, and Xinglin Zhou. «Fiber Bragg Grating-Based Three-Axis Vibration Sensor». In: *IEEE Sensors Journal* 21.22 (2021), pp. 25749–25757 (cit. on p. 27).

[14] Hui Wang and Qing-Hua Qin. *Methods of fundamental solutions in solid mechanics*. Elsevier, 2019 (cit. on p. 27).

[15] Rujun Wu, Bailin Zheng, Zhigang Liu, Pengfei He, and Yuegang Tan. «Analysis on strain transfer of a pasted FBG strain sensor». In: *Optik* 125.17 (2014), pp. 4924–4928 (cit. on p. 36).

[16] Guang Chen, Keqin Ding, Qibo Feng, Xinran Yin, and Fangxiong Tang. «Strain transfer mechanism of grating ends fiber Bragg grating for structural health monitoring». In: *Structural Durability & Health Monitoring* 13.3 (2019), p. 289 (cit. on p. 36).

[17] Tianliang Li, Yuegang Tan, Zude Zhou, Li Cai, and Ruiya Li. «Research on pasted FBG-based accelerometer's sensitization process method and its characteristics». In: *IEICE Electronics Express* (2015), pp. 12–20150583 (cit. on p. 36).

[18] S. Timoshenko. «Vibration Problems in Engineering». In: D. Van Nostrand Company, Inc., 1937. Chap. 1, pp. 85–86 (cit. on p. 40).